Eidgenössische Technische Hochschule Zürich
Swiss Federal Institute of Technology Zurich

Institute for
Dynamic Systems and Control
IDSC
Institut für Dynamische Systeme
und Regelungstechnik

DAIMLER

Achin Jain

Optimal Control of a Hybrid Electric Vehicle with an Electrically Assisted Turbocharger

Master Thesis

Institute for Dynamic Systems and Control
Swiss Federal Institute of Technology (ETH) Zurich

Supervision

Christian Naegele, Daimler AG
Pedro Macri-Lassus, Daimler AG
Dr. Tobias Nüesch, ETH Zurich

December 2014

IDSC-LG-TN-24

Preface

This work has been done as a master thesis at Daimler AG, Stuttgart in collaboration with the Institute for Dynamic Systems and Controls at ETH Zurich.

Working on this project has been a very enriching experience. In addition to gaining knowledge in the subject, I could learn the key lessons to conduct fruitful research. This has been possible because of a number people I associated with and I am very grateful to each one of them.

I would like to thank Prof. Dr. Christopher Onder and Prof. Dr. Lino Guzzella for being my faculty advisors at ETH and Pedro Macri-Lassus, my supervisor at Daimler, for giving me an excellent opportunity to be a part of Daimler Research and Development in Stuttgart. Besides, I would also like to thank Pedro for his invaluable guidance and lending me his expert knowledge, especially about the turbochargers, throughout the project. My thanks also goes to Christian Naegele, who has been my first contact person at Daimler, for assisting me whenever possible. Plenty of discussions with him have been very insightful. I would like to express my sincere gratitude towards my supervisor at ETH, Dr. Tobias Nüesch for his never-ending support, be it his regular feedback on my work or his assistance in many administrative issues. Tobias's already accomplished research work served as background tools and with its help I could save time and concentrate more on other essential aspects of the project.

Achin Jain

Contents

Zusammenfassung

In der vorliegenden Arbeit wird ein Hybridfahrzeug bestehend aus einem Ottomotor mit elektrisch unterstütztem Abgasturbolader (ATL) und einem Traktions-Elektromotor untersucht. Dabei liegt der Fokus auf der Eignung der elektrischen ATL-Unterstützung hinsichtlich Kraftstoffverbrauch und Fahrleistung. Der zweite Elektromotor zur Unterstützung des ATL hat eine direkte Verbindung zu dessen Welle und bietet dem System einen zusätzlichen Freiheitsgrad in der Betriebsstrategie. Die elektrische Energie kann entweder direkt zur Traktion oder zur Unterstützung des ATL eingesetzt werden. Die Aufgabe besteht in der optimalen Steuerung der Drehmomentverteilung zwischen Verbrennungsmotor und Traktions-Elektromotor sowie der Leistung des Elektromotors zur ATL -Unterstützung und der Getriebegangstufe.

Zunächst wird ein regelungstechnisches Modell für ein Hybridfahrzeug mit Turbomotor erstellt. Dazu werden verschiedene Methoden zur Modellierung des ATL-Verhaltens (Turboloch) untersucht. Hier zeigt ein kennfeldbasiertes Modell, das anhand von Messdaten kalibriert wird, die beste Übereinstimmung.

Um eine optimale Betriebsstrategie zu finden, wird die Methode der Dynamischen Programmierung eingesetzt. Die vorhandene elektrische Leistung ist begrenzt und wird auf beide Elektromotoren verteilt. Dabei wird analysiert wann die elektrische Unterstützung des Turboladers vorteilhaft ist. Hinsichtlich des Kraftstoffverbrauchs sind kaum und nur bei hohen Lastanforderungen Verbesserungen möglich. Der Einfluss auf die Fahrleistung ist deutlicher. Wird die elektrische Energie nicht zur Traktion sondern zur Unterstützung des ATL eingesetzt, erhöht sich das Beschleunigungsvermögen des Fahrzeugs signifikant.

Des Weiteren wurde die Beeinflussung der Betriebsstrategie durch Variation der Antriebsstrangkomponenten analysiert, besonders hinsichtlich der Fahrleistung. Für den Verbrennungsmotor wurde der Hubraum variiert und dabei der Turbolader angepasst, um die Nennleistung und das maximale Drehmoment gleich zu halten. Für den Traktionsmotor wurde die Nennleistung variiert. Die Variationen wurden durch theoretische Skalierung der Kennfelder der jeweiligen Komponenten erreicht. Die Untersuchungen zeigen, dass die Vorteile umgekehrt proportional zum Hubraum des Verbrennungsmotors und in geringerem Maße auch zur Nennleistung des Traktionsmotors sind.

Abstract

This thesis presents an investigation on suitability of using an electrically assisted turbocharger in a hybrid electric vehicle (HEV) with a turbocharged engine, based on fuel economy and acceleration performance. This system has two electric machines, traction motor and boost motor, and offers an additional control variable in energy management problem i.e. the amount of electrical boost (e-boost) to reduce turbolag. The task of an optimal controller now becomes manifold: deciding the torque split between engine and traction motor, the power of the boost motor and the gear number.

First, a control-oriented model of a parallel HEV with a turbocharged engine is derived based on first principles. After a series of investigations, a suitable method to model turbolag is proposed. It is based on a predefined map for permissible engine torque obtained through scattered interpolation of experimental measurements. The boost mechanism uses an electric motor coupled to the shaft of the turbocharger.

Dynamic Programming is used to solve the optimal control problem. In order to find out an optimal trade-off between the two on-board electric machines, optimal strategy is calculated with a constraint on maximum total electrical power. The circumstances in which it is advantageous to use a boost motor have been discussed. In the control problem with fuel minimization, the simulation results reveal that fuel consumption of an HEV without the e-boost can be reduced slightly by installing a boost mechanism only under high load requirements. The impact of e-boost on the acceleration performance of the vehicle is more prominent. Using a fraction of the total available electrical power, a boost motor can significantly reduce the time required to accelerate from an initial speed to a given final speed.

Further, the influence of powertrain component sizes on the operation strategy has been analyzed, specifically in the problem of maximizing acceleration performance. A theoretical research is done by scaling the engine displacement volume for different size of turbochargers keeping the maximum engine torque and power constant, and motor map for different nominal powers. The result indicates that the benefits are inversely proportional to the size of the engine as well as the nominal power of the traction motor. This dependence is stronger on the engine size and weaker on the motor power.

Nomenclature

Symbols

α	Inclination of road	[rad]
Δ	Change in a quantity	$[\cdot]$
$\dot{\mu}$	Normalized mass flow rate	$[^{kg}/_{s}]$
$\dot{\omega}$	Angular acceleration	$[^{rad}/_{s^2}]$
$\dot{m}$	Mass flow rate	$[^{kg}/_{s}]$
ϵ	A small number	$[-]$
η	Efficiency	$[-]$
Γ	Engine fuel consumption map	$[^{kg}/_{s}]$
γ	Gear ratio	$[-]$
Λ	Power map of motor	[W]
$\mathbb{R}$	Set of real numbers	$[-]$
M	Model	$[-]$
μ	Control policy, cost coefficient	$[-, -]$
Ω	Torque map based on engine and turbocharger speed	[Nm]
ω	Angular speed	$[^{rad}/_{s}]$
ϕ	Terminal cost in dynamic programming	$[-]$
π	Mathematical constant equal to 3.14	$[-]$
π	Pressure ratio	$[-]$
Ψ	Torque map based on engine speed and power	[Nm]
ρ	Density	$[^{kg}/_{m^3}]$
τ	Time constant	[s]
Θ	Moment of inertia	$[kgm^2]$
Υ	Permissible torque map	[Nm]

ϑ	Temperature	[K]
ξ	State of charge of battery	[−]
ζ	Torque split input	[−]
A	Area	[m^2]
a	Acceleration	[m/s^2]
C	Coefficient	[−]
cos	Cosine function	[·]
F	Force	[N]
f	State derivative	[·/s]
g	Acceleration due to gravity, state cost	[m/s^2, −]
H	Hamiltonian, heating value of fuel	[J/kg,-]
h	Nonlinear function describing evolution of speed	[m/s]
I	Current	[A]
i	Iteration number	[−]
J	Cost-to-go	[−]
l	Nonlinear function describing evolution of engine torque	[Nm]
m	Mass, number of control inputs	[kg, −]
N	Number of time steps, number of half rotations	[−, −]
n	Number, number of states	[−, −]
P	Power	[W]
p	Pressure, number of disturbances	[Pa, −]
Q	Charge	[Ah]
R	Resistance	[ohm]
r	Radius	[m]
sgn	Signum function	[·]
sin	Sine function	[·]
T	Torque, terminal time	[Nm,s]
t	Continuous time index	[s]
U	Voltage, range of inputs	[V, ·]
u	Model input	[·]

V	Volume	$[\mathrm{m}^3]$
v	Velocity	$[\mathrm{m/s}]$
W	Range of disturbances	$[\cdot]$
w	Model disturbance	$[\cdot]$
X	Range of states	$[\cdot]$
x	Model State	$[\cdot]$

Indicies

air	Air
aux	Auxiliary
des	Desired
ex	Exhaust manifold
fr	Front
idle	Engine in idle mode
im	Intake manifold
init	Initial
in	Inlet port
max	Maximum of a quantity
min	Minimum of a quantity
na	Naturally aspirated
out	Outlet port
a	Aerodynamic
ac	Acceleration
amb	Ambient
b	Battery
c	Compressor
cb	Coulomb
chg	Charging
cs	Charge sustaining
d	Displacement, drag
dis	Discharging

e	Engine
g	Gear, gravity
gb	Gearbox
k	Discrete time index
l	Lower
m	Motor
me	Mean effective
oc	Open circuit
r	Rolling
s	Sampling time
t	Traction, turbine
tc	Turbocharger
v	Vehicle
w	Wheel

Acronyms and Abbreviations

A-ECMS	Adaptive ECMS
BM	Boost Motor
BSFC	Brake Specific Fuel Consumption
BT	Battery
C	Compressor
CL	Clutch
Cvx-DP	Convex optimization with Dynamic Programming
DC	Driving Cycle
DP	Dynamic Programming
ECMS	Equivalent Consumption Minimization Strategy
EGR	Exhaust Gas Regeneration
EMS	Energy Management Strategy
EPA	Electric Power Assist
ETC	Electric Turbocompounding
ETC-ICE	Electric Turbocompounding coupled to Internal Combustion Engine

ETC-TC	Electric Turbocompounding coupled to Turbocharger
f-ECMS	Fuzzy ECMS
HEV	Hybrid Electric Vehicle
ICE	Internal Combustion Engine
MPC-DP	Model Predictive Control with Dynamic Programming
MTC	Mechanical Turbocompounding
MVM	Mean Value Modeling
NEDC	New European Driving Cycle
NFDC	New Fast Driving Cycle
P1	Parallel 1
PMP	Pontryagin's Minimum Principle
S-DP	Stochastic Dynamic Programming
SoC	State of Charge
T	Turbine
T-ECMS	Telemetry ECMS
TM	Traction Motor
TPA	Turbo Power Assist
VGT	Variable Geometry Turbocharger
WLTC	Worldwide harmonized Light vehicles Test Cycle

Chapter 1

Introduction

Fuels based on fossils are unquestionably the best on-board energy sources in automobiles in terms of energy density and refueling time [22]. However, their use is not sustainable and is one of the reasons of growing environmental concerns. This poses two prime challenges in a conventional vehicle propelled with hydrocarbon based fuels: improving the fuel economy and reducing the emissions. Many solutions have been proposed to improve the fuel efficiency, including turbocharging [60] and hybridization [46].

Besides, driveability is another important measure of performance which assesses vehicle's speed and acceleration capabilities. It also quantifies driving comfort in the form of frequency of engine on-offs, frequency of gear shifts etc. While the passenger vehicles should be able to meet the basic acceleration demands in a driving cycle with minimal fuel requirements, the acceleration performance is given more importance over fuel consumption in racing sports. The most common way to improve the acceleration performance of a turbocharged engine is by means of electrical assist which ensures extra power as well as high acceleration [29].

The goal of this thesis is to evaluate the suitability of using an electrically assisted turbocharger in a parallel hybrid electric vehicle and analyze the performance with respect to fuel consumption and acceleration performance. In the following sections, a comprehensive literature review on this technology is presented.

1.1 Turbocharging

In a conventional vehicle, without exhaust heat recovery, roughly 30-40% of energy is lost in exhaust gas [10]. Only few methods are based on utilizing the wasted energy in the exhaust gas, for example bottoming cycles [51, 16], thermoelectric generation [3, 36] and turbocharging. And of these, turbocharging is a better alternative because of limited availibility of thermoelectric material and size, weight, cost and durability issues associated with the bottoming cycles [25]. A turbocharger helps to boost the pressure of air entering the engine by deriving energy from the exhaust gas which is otherwise wasted. It further al-

lows the engine to be downsized and thus a turbocharged engine performs more efficiently, thereby reducing the fuel consumption and the emissions.

In a classical turbocharger, a waste gate is used at high engine speeds to regulate excess boost pressure by limiting the amount of exhaust gas through the turbine. Clearly, when the waste gate is open, some potential power in the exhaust gas is lost. A Variable Geometry Turbocharger (VGT) overcomes this drawback by changing the turbine geometry such that the turbocharger can be used in a wide zone of engine speeds. The performance with respect to fuel economy and emissions can be further improved with a well known technology called turbocompounding. It uses multiple turbines/compressors and/or motor/generators depending upon the configuration. Turbocompunding can additionally recover wasted energy downstream of the turbine of the conventional turbocharger and can possibly eliminate the need of waste gates. On the basis of topology, turbocompounding may be categorized into two types: Electric Turbocompounding (ETC), and Mechanical Turbocompounding (MTC).

Turbocompounding is sometimes also referred to as turbo power assist (TPA), since it assists the engine with external power mechanically or electrically. Several variants of mechanical and electrical turbocompounding have been proposed in the literature [7]. ETC consists of a motor/generator directly coupled to the crank shaft (ETC-ICE) or to the shaft of the turbocharger (ETC-TC), making it compact in the latter case. Additionally, it may also use a second turbine which is connected to the generator. Such an arrangement is also called Electric Power Assist (EPA). MTC employs a second turbine which is connected to the engine crank shaft mechanically. Recovered energy in ETC can be stored in a battery for a later use, as decided by the control strategy while this doesn't hold true for MTC. Thus, ETC can also be used to power auxiliary devices.

ETC has proven to be fuel efficient and less emissive in heavy duty engines while the technology is still immature in small displacement engines. As much as 10% reduction in fuel consumption is possible with ETC in heavy duty diesel engines depending upon driving cycles [8, 24, 25, 55]. Also, ETC-TC can be more effective over its mechanical counterpart because it can exploit the advantage of operating at more efficient points while this is a restriction in the mechanical case because of mechanical coupling with crankshaft [19, 55]. Turbocompounding has also shown an adverse effect on small displacement engines. This is mainly because, it causes high back pressures in the exhaust and as a result the engine performs less efficiently [14, 26]. However, on-board energy management strategies can provide further scope of improvement in this class of engines [1].

ETC also improves the response time of the turbocharger. Both designs of the turbocharger (with and without VGT) suffer from an inherent disadvantage of turbolag, although less in VGT because performance can be optimized with respect to this characteristic [56]. Electric machine or the boost motor used in ETC is often reversible. In motor mode, it accelerates the turbocharger (or crank shaft) and in generator mode, it stores the energy for future use. Electric power assist helps to alleviate the turbo lag, an advantage over both classical turbocharging and mechanical compounding [15, 39, 44].

The drawbacks of turbocompounding include exhaust back pressure which causes pumping losses [24] and potentially, sudden deceleration of the turbocharger which may eventually lead to compressor surge [54].

Nevertheless, turbocompounding is an attractive technology for an efficient propulsion, with regards to both fuel consumption and acceleration response, simultaneously. It is also evident that ETC can be more efficient than MTC because of the mechanical coupling constraint in MTC and can provide more freedom in defining control strategies in HEVs as the new control input in the form of electrical boost (e-boost) can be controlled independently.

1.2 Hybridization

With availability of another on-board energy source, a hybrid electric vehicle (HEV) can potentially decrease both fuel consumption and emissions. In particular, an HEV can operate at more efficient engine set points and the engine can be downsized while fulfilling the same maximum power requirements [22]. Other benefits in HEVs come from recuperation, energy management between the two power sources and possibly by reduction in clutching losses. A method to estimate fuel consumption benefits in HEVs can be found in [43].

Energy Management Strategy (EMS) or the so called Supervisory Control Strategy forms the heart of an HEV design. EMS can be classified into two groups: rule-based control strategies/heuristic EMS and numerical optimization-based control strategies which can be applied offline or online. A comprehensive review of EMS in HEVs can be found in [46]. The role of EMS is to decide the optimal power split between ICE and electric source(s) in order reduce fuel consumption or/and improve driving performance while satisfying the power demands of the vehicle. In the presence of electrical boosting, EMS must also decide the amount of e-boost i.e. the power of the boost motor in ETC.

In early studies, theoretical benefits of turbocompounding with turbocharged HEV were estimated [11, 49, 7]. Through scaling of data from the independent technologies like EPA, turbocharging and hybrid electric powertrains, it has been shown that assisted turbocharging in light hybrids can achieve same benefits as in full hybrids [49]. The control strategies for optimizing the performance of e-boost in HEVs has not advanced either. For example, heuristics-based boost control has been used in [57]. Equivalent Consumption Minimization Strategy (ECMS) has been employed in [5] to control the turbocharged HEV. However, in this study, electric boost is not controlled independently. In [33], optimal control has been applied to maximize the acceleration performance with ETC-TC applied to a conventional turbocharged engine. The methodology used here is closely linked to optimal EMS in HEVs. This serves as a motivation to explore the benefits of the two technologies combined together. In a more recent study, ETC with a combined hybrid has been analyzed in detail [61]. A live example of this technology is seen in the 2014 Formula One season [53].

1.3 Objective

In the above literature review, potential benefits of e-boost in conventional vehicles are clearly evident in fuel economy as well as acceleration performance. However, energy management in HEVs with an additional electric motor for boost control needs more investigation and there is a need to obtain simple modeling tools, and a systematic approach to deal with the problem. This thesis is an attempt in this direction. In particular, the thesis focuses on the following aspects of this problem:

1. Developing a simple yet authentic control-oriented model of a parallel hybrid electric vehicle equipped with an electrically assisted turbocharger,

2. Finding a suitable solution method for the optimal control problem,

3. Calculating an optimal control strategy for this model by minimizing fuel consumption and maximizing acceleration performance, and

4. Analyzing the influence of different sizes of powertrain components on the control strategy.

Control strategies for the aforesaid objectives will be calculated separately. The problem concerning the fuel consumption is explained in Fig. 1.1. The mass of fuel required to drive this particular driving cycle in pure ICE mode can be reduced by hybridization. The objective here is to analyze if the fuel consumption can be further reduced in a charge-sustaining operation, if at all, by using a motor to assist the turbocharger in the existing hybrid setup while not violating the same limit on maximum electrical power. The optimal fuel consumption in an HEV with an e-boost can never exceed the consumption in an HEV without it, otherwise the optimal strategy would be not to use the boost motor in which case the consumption would be same as in HEV without an e-boost.

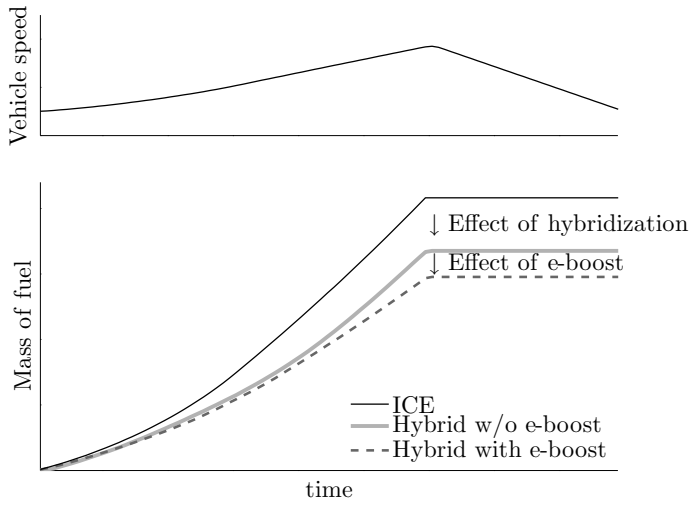

Figure 1.1: Problem of minimizing fuel consumption. The initial and final state of charge of battery is same in all the cases.

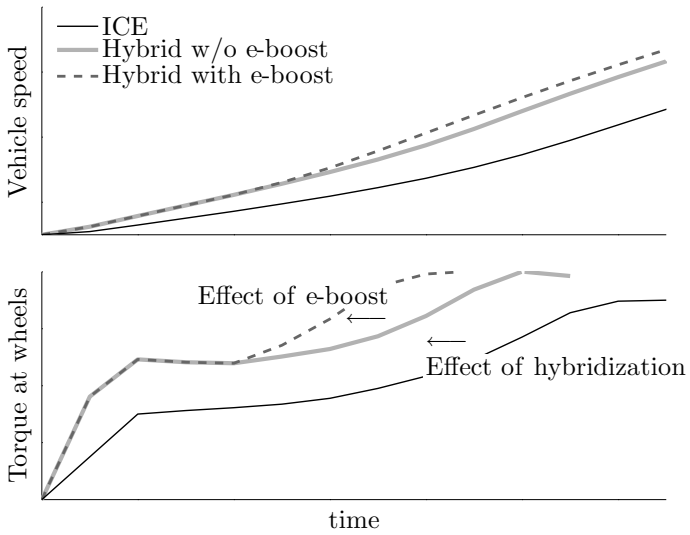

Figure 1.2: Problem of minimizing time required to accelerate from a given speed to a final speed or maximizing speed at the end.

The next objective is to study the influence of the boost motor on acceleration response at full throttle. It is same as maximizing the speed at the end of a mission or minimizing the time required to achieve a reference torque, for example the maximum engine torque. It is illustrated in Fig. 1.2. In general, an HEV can accelerate faster than a conventional vehicle with the same turbocharged ICE because the motor torque is instantaneously achieved and more power is delivered at the wheels. Now, in the presence of a boost motor, the turbolag can be overcome to further improve the acceleration response and achieve a higher vehicle speed at the end. Under the constraint of same total electrical power, in the optimal scenario, the performance of an HEV with an e-boost cannot be worse than an HEV without it.

1.4 Report Layout

In Chap. 2, a control-oriented model of a P1 hybrid with a turbocharged engine is derived. A simple method for modeling the turbolag and the boost mechanism is proposed. Chap. 3 discusses a framework to solve the optimal control problem and optimize the control strategy for two different objectives, viz. minimizing fuel consumption and maximizing acceleration performance. In Chap. 4, the effects of powertrain components' size on the optimal strategy are analyzed. Finally, the thesis is concluded with a discussion on the achieved results and future prospects of the project.

Chapter 2

Modeling

This chapter discusses the modeling of various components of an electrically assisted turbocharged parallel hybrid powertrain. For this study, the so called P1 hybrid topology has been considered. The parameters of the reference model have been adopted from Mercedes-Benz E-Class. These have been scaled appropriately for further studying the influence of component sizes on the control strategy.

The schematic diagram of a P1 HEV is shown in Fig. 2.1. The vehicle is propelled at rear wheels. The traction motor (TM) and the internal combustion engine (ICE) are connected to the drivetrain shaft through a torque coupler which can be decoupled from the drivetrain using the clutch (CL). The boost motor (BM) is attached to the turbocharger shaft which accelerates both compressor (C) and turbine (T) as commanded by the control strategy. Both the motors are connected to the battery (BT). TM is a reversible electric machine which can also be used to recuperate energy while BM can only use energy from BT to assist the ICE. The vehicle is incapable of a pure electric drive. The quasistatic-models or the backward models described in the following sections have been adapted from [22].

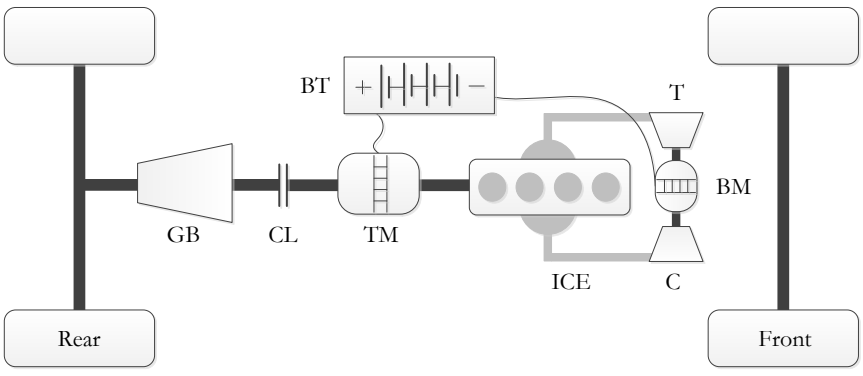

Figure 2.1: Topology of a P1 hybrid electric vehicle.

2.1 Vehicle Dynamics

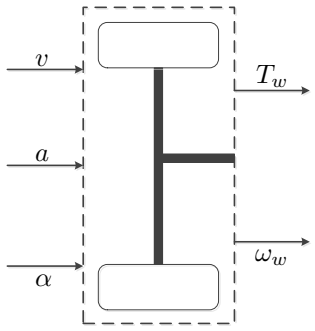

Figure 2.2: Quasistatic model of vehicle dynamics.

Quasistatic model for vehicle dynamics is shown in Fig. 2.2. Velocity and acceleration of the vehicle, and driving slope are known from the diving cycle. Torque required at wheels and rotation speed of the wheels are estimated.

Traction force F_t required to drive a vehicle can be expressed as follows:

$$F_t = F_{ac} + F_a + F_r + F_g, \tag{2.1}$$

where F_{ac} is the acceleration term given by

$$F_{ac} = (m_v + m_r)\ a, \tag{2.2}$$

m_v is the mass of the vehicle including the engine, motors, battery and gear box, v the velocity of the vehicle and a the acceleration of the vehicle. The rotational mass m_r is a function of gear ratio γ , moment of inertia of wheels Θ_w and of the engine Θ_e:

$$m_r = \frac{1}{r_w^2}\ \Theta_w + \frac{\gamma^2}{r_w^2}\ \Theta_e. \tag{2.3}$$

F_a represents the aerodynamic losses defined by

$$F_a = \frac{1}{2}\ \rho_{\text{air}}\ A_{\text{fr}}\ C_d\ v^2, \tag{2.4}$$

where ρ_{air} is the density of the air, A_{fr} the frontal area of the car and C_d the aerodynamic drag coefficient.

F_r accounts for the rolling fiction losses. It is modeled according to the relation

$$F_r = m_v\ C_r\ g\ cos(\alpha), \tag{2.5}$$

where C_r is the rolling friction coefficient, g the acceleration due to gravity and α the slope of the driving path.

F_g represents the contribution of the gravity, given by

$$F_g = m_v \; g \; sin(\alpha). \tag{2.6}$$

Equation (2.1) can be now used to define torque demand at wheels T_w as follows:

$$T_w = r_w \; (F_{ac} + F_a + F_r + F_g). \tag{2.7}$$

Here, r_w is the radius of the wheels. Finally, the rotation speed of the wheels can be expressed as

$$\omega_w = \frac{v}{r_w}. \tag{2.8}$$

2.2 Gearbox

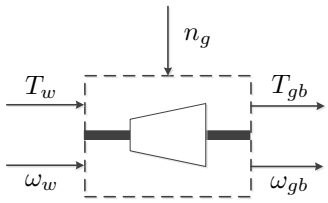

Figure 2.3: Quasistatic model of a gearbox.

The vehicle under consideration has 7 forward gears. The outputs of the vehicle dynamics model are the inputs to the gearbox model (Fig. 2.3). The rotational speed of the drivetrain shaft on the engine side of the gearbox ω_{gb} is related to the input speed ω_w as follows:

$$\omega_{gb} = \gamma \; \omega_w. \tag{2.9}$$

The torque on the engine side of the gearbox T_{gb} can be expressed as

$$T_{gb} = \frac{T_w}{\gamma} \; \eta_{gb}^{-sgn(T_w)}. \tag{2.10}$$

where T_w is negative under recuperation and positive under traction. sgn is the signum function and γ is the gear ratio. The corresponding gear number n_g is decided by the control strategy. The gearbox is assumed to have a constant mechanical efficiency η_{gb}.

2.3 Torque Coupler

The electric machine TM is coupled to the drivetrain directly, without any speed reduction. Thus, the traction motor and the engine rotate at the same speed.

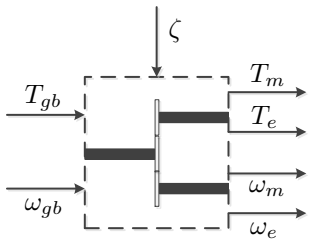

Figure 2.4: Quasistatic model of a torque coupler.

The engine speed ω_e and traction motor speed ω_m can be expressed in terms of ω_{gb} as

$$\omega_e = \omega_m = \begin{cases} \omega_{gb} & \text{if clutch is not slipping, and} \\ \max\left(\omega_{e,\text{idle}}, \omega_{gb}\right) & \text{if clutch is slipping} \end{cases} \tag{2.11}$$

The energy balance across the coupler gives a relation between the torque produced by the traction motor T_m and the engine torque T_e,

$$T_{gb} = T_m + T_e \tag{2.12}$$

$$T_m = \zeta\, T_{gb}. \tag{2.13}$$

The torque split ζ is decided by the control strategy. It lies between $\zeta_{\min} = -1$ and $\zeta_{\max} = 1$. If the battery is sufficiently charged, then the generator might not be able to recuperate the entire energy. Under these conditions, the extra energy is dissipated in friction brakes. It is assumed that there are no energy losses in both the torque coupler and the clutch.

2.4 Electric Motor/Generator

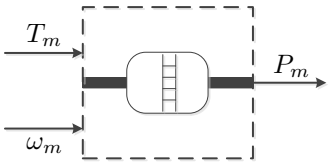

Figure 2.5: Quasistatic model of an electric motor/generator.

The reference electric motor/generator (referred as the traction motor to distinguish it from the boost motor) has a maximum power rating of 20 kW. Once the torque split is known from the control strategy, the motor torque is known

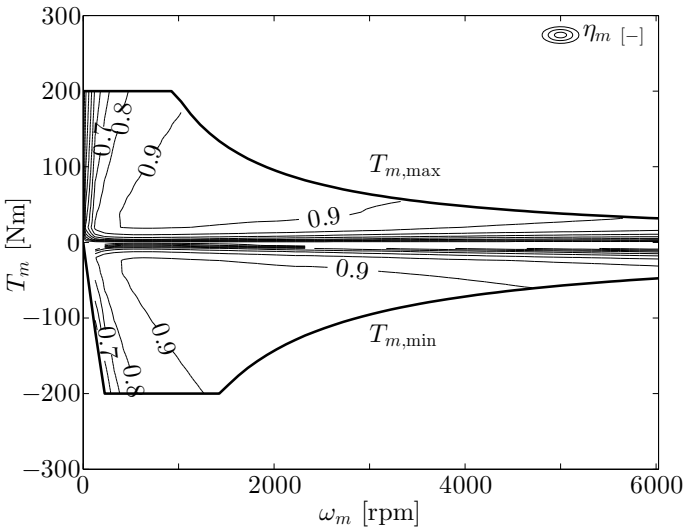

Figure 2.6: Torque-speed characteristic of an electric motor/generator. $T_{m,\max}$ and $T_{m,\min}$ are the maximum motor and generator torque, respectively.

in Fig. 2.5. The power P_m as a function of the motor speed ω_m and the motor torque T_m is known through a power map:

$$P_m = \Lambda(\omega_m, T_m). \tag{2.14}$$

Because of energy losses in the motor,

$$P_m \geq sgn(T_m) \ |\omega_m \ T_m| \,. \tag{2.15}$$

It works in motor mode when $T_m \geq 0$ and in generator mode when $T_m < 0$. The torque-speed characteristic of the motor, along with the efficiency η_m, is shown in Fig. 2.6.

The maximum motor and generator torque, $T_{m,\max}$ and $T_{m,\min}$ respectively, depend on the speed:

$$T_{m,\min}(\omega_m) \leq T_m(\omega_m) \leq T_{m,\max}(\omega_m). \tag{2.16}$$

2.5 Internal Combustion Engine

The reference turbocharged engine has a power rating of 155 kW and provides maximum torque of 350 Nm. The ICE must operate at the desired set point (ω_e, T_e) as calculated in (2.11) and (2.13). The fuel consumption is then calculated using a map based on measurements at stationary operating conditions as a function of the mean effective pressure p_{me} and the engine speed ω_e,

$$\dot{m}_f = \Gamma(\omega_e, p_{me}). \tag{2.17}$$

The mean effective pressure is related to the engine torque by the expression

$$p_{me} = \frac{N \ \pi \ T_e}{V_d}, \tag{2.18}$$

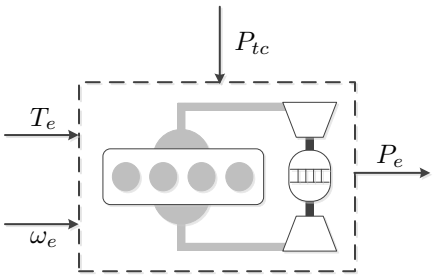

Figure 2.7: Quasistatic model of an electrically assisted turbocharged ICE.

where $N = 4$ is used for a four stroke engine and V_d is the displacement volume of the engine. The map for brake specific fuel consumption (BSFC) along with the engine torque at full-load operation or the maximum engine torque $T_{e,\max}$ is shown in Fig. 2.8. $T_{e,\min}$ is the drag torque which accounts for all the mechanical losses and $T_{e,0\text{comb}}$ is the drag torque when combustion is off. Switching between $T_{e,\min}$ and $T_{e,0\text{comb}}$ is digital.

For the purpose of controls in HEVs, mean value modeling (MVM) of ICE is not necessary and use of stationary maps like in Fig. 2.6 and Fig. 2.8 suffices. But to study the effects of turbolag and boost motor in a turbocharged engine, the model must be more complex. In particular, it should also depend on variables like inlet air pressure and temperature, exhaust air pressure and temperature, turbocharger speed and so on. MVM is one approach to deal with this [18]. The

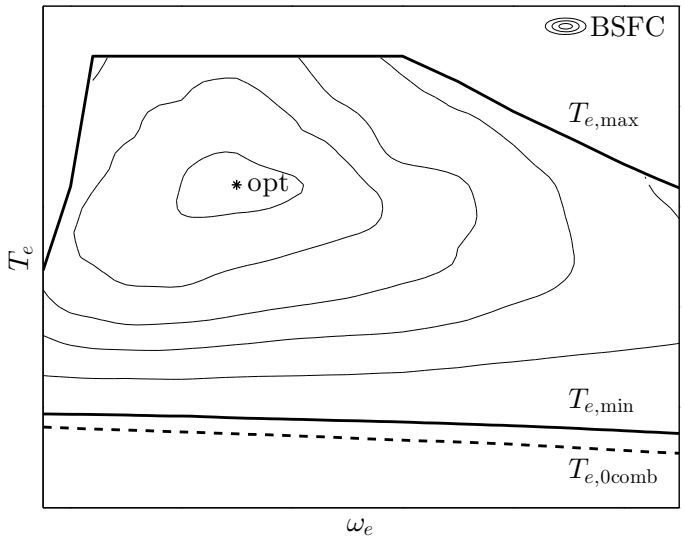

Figure 2.8: Torque and efficiency map of a turbocharged gasoline engine.

highly complex model in this study considers each engine component and has 13 states. Even if the mean value model is simplified, as in [32] where the number of states are 7, the model is dependent on an engine temperature rise map and a volumetric efficiency map, in addition to the turbocharger maps, which are not easily available. The problem size is further reduced by getting rid of the variables with slow dynamics in [50]. Nevertheless, the approach with MVM is not trivial and can also be time consuming. In this thesis, an alternate and simpler way to model the turbolag behavior is proposed. This control-oriented model is also easily adaptable to the electric boost mechanism which is discussed in the last part of this section.

2.5.1 Turbocharger

The fundamental definitions in this section have been adopted from [21]. Many reasonable assumptions have been made while modeling the turbocharger. For instance, throttle, intercooler, intake manifold, exhaust manifold and exhaust gas regeneration (EGR) have not been modeled. Of all, the key assumptions are listed below:

A1: Combustion is always carried out at stoichiometric air fuel ratio.

A2: Pressure and temperature at the outlet port of compressor $(p_{c,\text{out}}, \vartheta_{c,\text{out}})$ are same as that in intake manifold (p_{im}, ϑ_{im}).

A3: Mass flow rate at the outlet port of compressor $\dot{\mu}_c$ is same as mass flow rate of air entering the engine $\dot{m}_{\text{air}}$.

A4: Engine operates at a constant volumetric efficiency η_v under stationary conditions.

A5: Pressure and temperature at the inlet port of compressor $(p_{c,\text{in}}, \vartheta_{c,\text{in}})$ are at ambient conditions $(p_{amb}, \vartheta_{amb})$.

Under the assumption A1, the mass flow rate of air can be computed from the fuel mass flow rate (2.17) as:

$$\dot{m}_{\text{air}} = \lambda^* \, \dot{m}_f, \tag{2.19}$$

where $\lambda^* = 14.7$ is the stoichiometric air fuel ratio. Under the assumptions A2-A4, the mass flow rate of air-fuel mixture entering the engine can be related to the pressure of the mixture in intake manifold by the equation

$$\dot{m}_{\text{air}} + \dot{m}_f = \frac{1}{2} \, \frac{p_{im}}{R \, \vartheta_{im}} \, \eta_v \, V_d \, \frac{\omega_e}{2 \, \pi}. \tag{2.20}$$

The ratio of the pressure of the intake mixture p_{im} calculated from the above equation and the ambient pressure P_{amb} is shown in the Fig. 2.9. Under the assumption A5, this ratio is same as the pressure ratio Π_c across the compressor. The turbocharger is required only in the region where $\Pi_c > 1$.

A fluid dynamic compressor is causally described by 3 inputs: the pressures at the compressor inlet and outlet ports, the compressor rotational speed and the temperature at the compressor inlet port. Using these, the mass flow rate

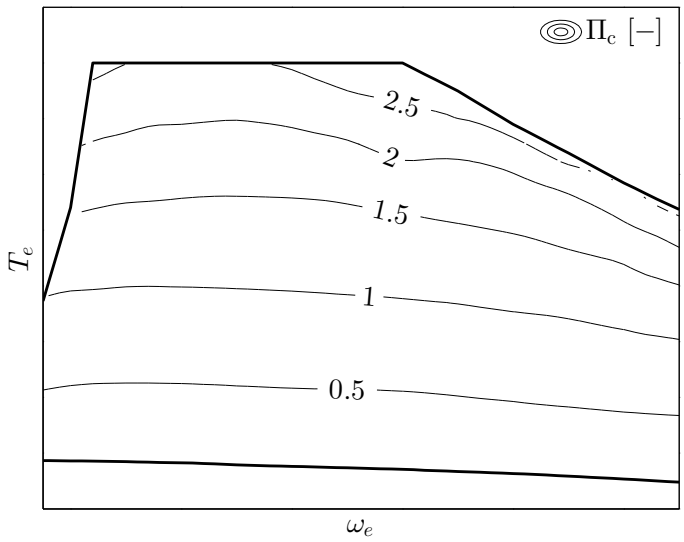

Figure 2.9: Pressure ratio of air in the intake manifold.

through the compressor $\dot{\mu}_c$ can be calculated. All these variables for the turbocharger of the reference engine are available in form of measurements. Due to practical limitations, the data cannot be measured over a wide range of inputs. Thus, a compressor map must be obtained by regression of the available data. The compressor map of the considered turbocharger obtained by fitting method [27] is shown in Fig. 2.10.

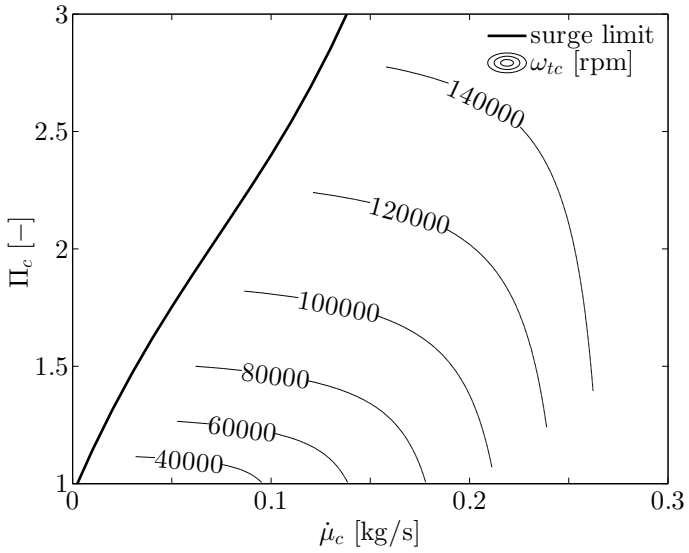

Figure 2.10: Compressor map.

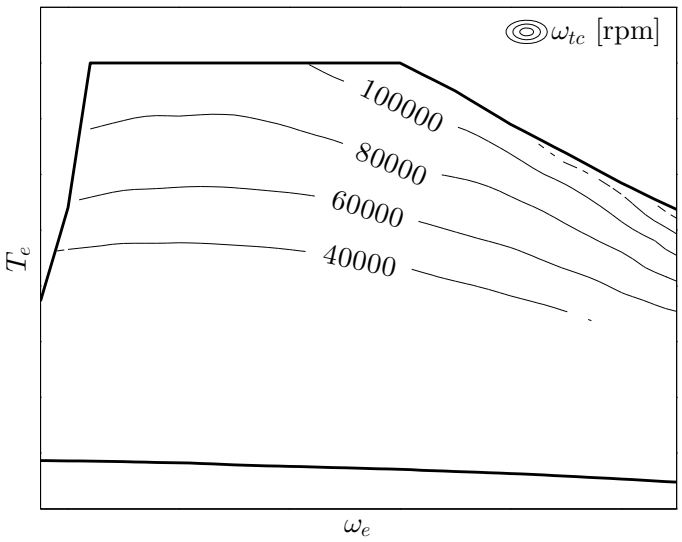

Figure 2.11: Turbocharger speed for all engine operating points.

For quasistatic modeling, the mass flow through the compressor and the pressure ratio across the compressor have been used as inputs for calculation of the turbocharger speed by interpolation of the compressor map. The turbocharger speed for all the operating points has been shown in Fig. 2.11.

To this end, the variables like mass flow rate of air, pressure ratio in intake manifold and turbocharger speed are known for all the operating points in the engine map.

2.5.2 Turbolag

Due to turbolag in a turbocharged engine, the torque delivered by the engine cannot be increased beyond a limit even if the desired torque is higher. This restriction is posed by the inertia of the turbocharger (TC) which must be accelerated in order to meet the higher demands. A proven solution to this problem is the use of a boost motor which uses energy from the battery to accelerate the TC whenever required [34]. In order to approximate the behavior of turbolag in a real engine, a series of methods were investigated for their accuracy. All of these have been presented here and finally a fairly accurate way to model the turbolag is proposed.

Turbolag is a strong function of the torque that the engine delivers at the previous time instant $t-1$, if the current time instant is denoted by t. Therefore, the engine torque must be one of the states in the control problem. Note that time t is used in a discrete sense here. In the following models, $T_{e,\max}$ refers to the maximum engine torque as defined in Fig. 2.8. A new limit on this torque, that arises due to turbolag, is defined by $\hat{T}_{e,\max}$.

MODEL I: Approximation of First Order System

The simplest and a very intuitive model is based on an affine constraint that limits the maximum achievable engine torque $\hat{T}_{e,\max}(t)$ depending upon the engine torque at the previous time step $T_e(t-1)$:

$$\hat{T}_{e,\max}(t) = \min\left\{T_e(t-1) + \Delta T, T_{e,\max}(t)\right\}, \tag{2.21a}$$

$$\Delta T = T_s \left(\frac{T_{e,\max}(t) - T_{e,\mathrm{na}}(t)}{2\tau}\right). \tag{2.21b}$$

In this model, a new limit of the maximum engine torque is defined which accounts for the turbolag. It is based on an approximation of a first order process with time constant τ. Here, the naturally aspirated torque $T_{e,\mathrm{na}}$ is defined by $\Pi_c = 1$, see Fig. 2.9. $T_{e,\mathrm{na}}$ can almost be instantaneously achieved with a small lag of the order of 200 ms. T_s is the sampling time of discretization and ΔT is defined as the permissible torque change in a sampling time. This approach is graphically illustrated in Fig. 2.12. In the following text, $T_e(t-1)$ is defined as the reference point of ΔT.

Although, this approach works well at low engine speeds, it fails to approximate the behavior of a real engine at high engine speeds. In particular, when high engine speed is accompanied by gear upshifts, the engine speed falls down but the turbocharger still rotates at high speed and significantly low turbolag is observed in practice. Model (2.21) fails to capture this effect. This result is an indication that the constraint on maximum torque should be dependent on turbocharger speed as well. Another drawback with this approach is that the maximum engine torque (Fig. 2.8) varies significantly with the engine speed. Hence, the time constant should also be a function of the engine speed.

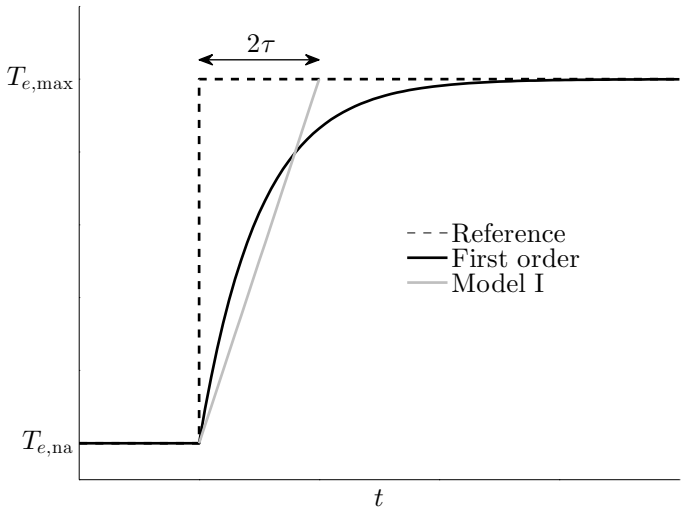

Figure 2.12: Model I: model of turbolag based on first order process. The slope of the model is used to calculate ΔT.

MODEL II: Dependence on Turbocharger Speed

A plausible solution to the aforesaid problem is that the reference for the permissible torque change at time t should be set such that the turbocharger speed at that time is equal to $\omega_{tc}(t-1)$. During a gear upshift, when the speed of the engine reduces, very low or almost no turbolag is experienced because the turbocharger still rotates at higher speed. Therefore, a new reference point $\hat{T}_e(t-1)$ is calculated such that after gear shifting (engine speed would be $\omega_e(t)$), the speed of the turbocharger is same as before:

$$\hat{T}_e(t-1) = \Omega(\omega_e(t), \omega_{tc}(t-1)), \tag{2.22a}$$

where

$$\Omega : (\omega_e, \omega_{tc}) \to T_e \tag{2.22b}$$

is obtained by inverting Fig. 2.11. This model is graphically represented in Fig. 2.13. Because $\hat{T}_e(t-1)$ is greater than $T_e(t-1)$, with same ΔT, it is possible to achieve higher torque with the new model during gear upshifts. Thus, the constraint (2.21) can be rewritten as

$$\hat{T}_{e,\max}(t) = \min\left\{\hat{T}_e(t-1) + \Delta T, T_{e,\max}(t)\right\}, \tag{2.23a}$$

$$\Delta T = T_s \left(\frac{T_{e,\max}(t) - T_{e,\mathrm{na}}(t)}{2\tau}\right). \tag{2.23b}$$

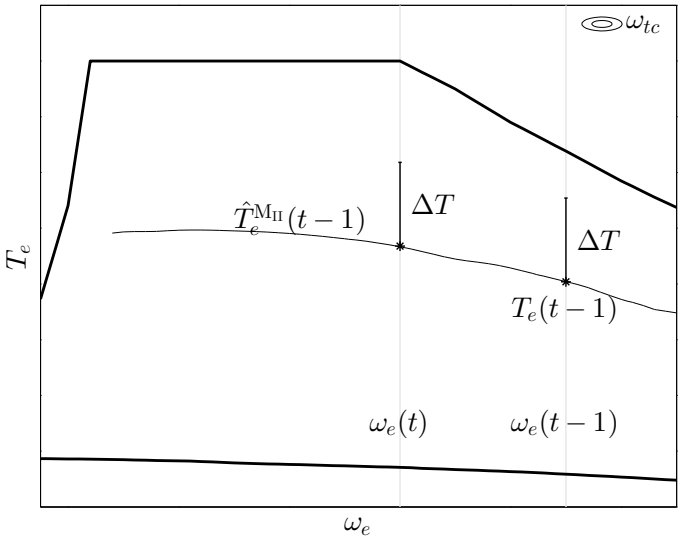

Figure 2.13: Mapping of Ω in Model II, shown in comparison with Model I. In Model II, the reference point is recalculated at the same turbocharger speed but at new engine speed. For the same ΔT, Model II results in higher $\hat{T}_{e,\max}$.

Simulation Environment for Testing

Model II was tested through a simulation under full-load conditions. This simulation environment has also been used later to test the models in the next sections. The vehicle is initially running at 8 kmph in the first gear. This speed has been chosen such that the corresponding engine speed is above the idling speed. The acceleration pedal is fully depressed and the vehicle tries to accelerate as fast as possible. The torque demand in this setup is set at maximum which enables us to observe the turbolag very distinctly. Moreover, the vehicle is run in pure ICE mode. Sampling time in this simulation is 0.1 s.

It is observed that there still exists unusual turbolag during gear upshifts at high speeds. Typically at high engine speeds, the waste gate lets out some amount of the exhaust gas which allows the turbocharger to maintain the same speed as before but with a lower mass flow rate. In the method described above, the interpolation of the turbocharger speed is based on how much mass flow is entering the engine (see Sec. 2.5.1). So, the lost mass flow rate has not been considered. Thus, it is reasonable to say that the turbocharger speed at high engine speed should be lower than obtained (because some mass flow is released) which would make the contours even steeper at high engine speeds. Hence, in this region, the turbocharger speed contours are expected to be parallel to the engine isopower curves. As a next step, this model is further modified by considering its dependence on the engine isopower curve.

MODEL III: Dependence on Isopower Curve

The reference point is now defined by isopower lines of the engine instead of the isospeed lines of the turbocharger. Hence,

$$\hat{T}_e(t-1) = \Psi(\omega_e(t), P_e(t-1)), \tag{2.24a}$$

where

$$P_e(t-1) = \omega_e(t-1)\ T_e(t-1) \text{ and } \Psi : (\omega_e, P_e) \to T_e. \tag{2.24b}$$

The constraint (2.21) is remodified as

$$\hat{T}_{e,\max}(t) = \min\left\{\hat{T}_e(t-1) + \Delta T, T_{e,\max}(t)\right\}, \tag{2.25a}$$

$$\Delta T = \frac{\Delta P}{\omega_e(t)}, \tag{2.25b}$$

where ΔP is the permissible power in a sampling time. The model has been graphically explained in Fig. 2.14.

The limit of the maximum engine torque in model III $\hat{T}^{\mathrm{M_{III}}}_{e,\max}$ is even more than that in model II ($\hat{T}^{\mathrm{M_{II}}}_{e,\max}$) which eliminates turbolag which was earlier observed during gear upshifts. An issue that still needs to be resolved is the dependence of permissible power on the engine speed. Infact, it is evident that at lower engine speeds, the permissible power must be lower because isopower lines are

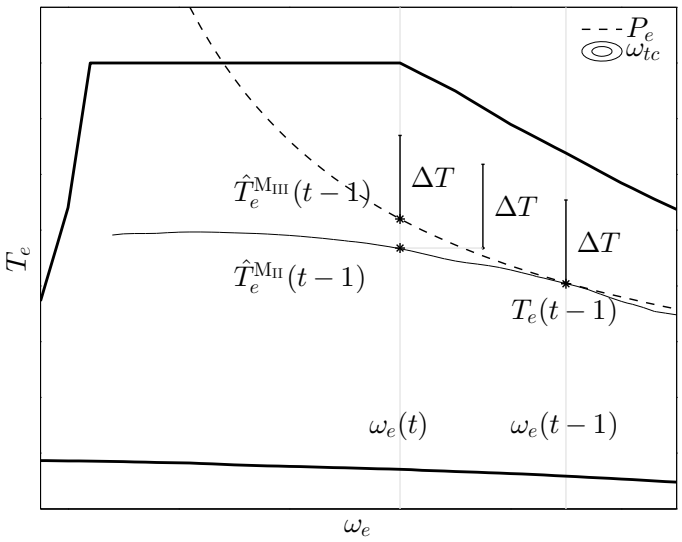

Figure 2.14: Mapping of Ψ in Model III, shown in comparison with Model I and Model II. The reference point in Model III corresponds to the engine power at previous time step. For the same ΔT, Model III results in the highest $\hat{T}_{e,\max}$.

very steep. Even a low ΔP results in much higher $\hat{T}_{e,\max}$. This eventually leads to very early gear upshifts while running the vehicle in the same simulation environment but now in a hybrid mode.

Fig. 2.15 exhibits this behavior. It particularly happens when the permissible

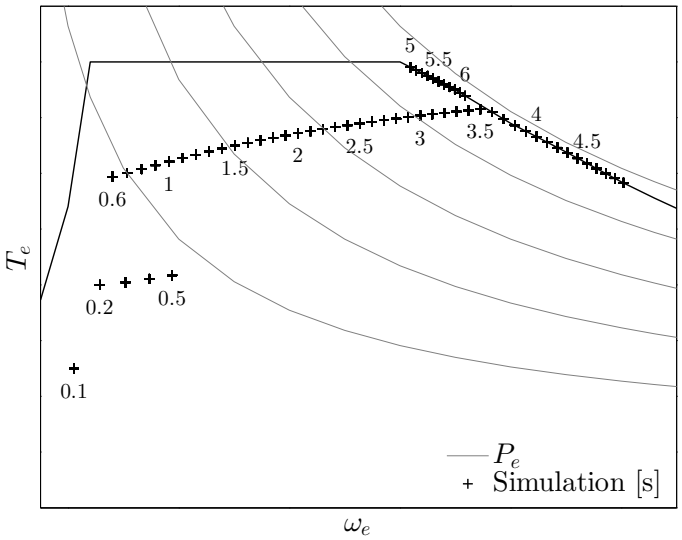

Figure 2.15: Early gear upshift as observed in Model III with constant permissible power.

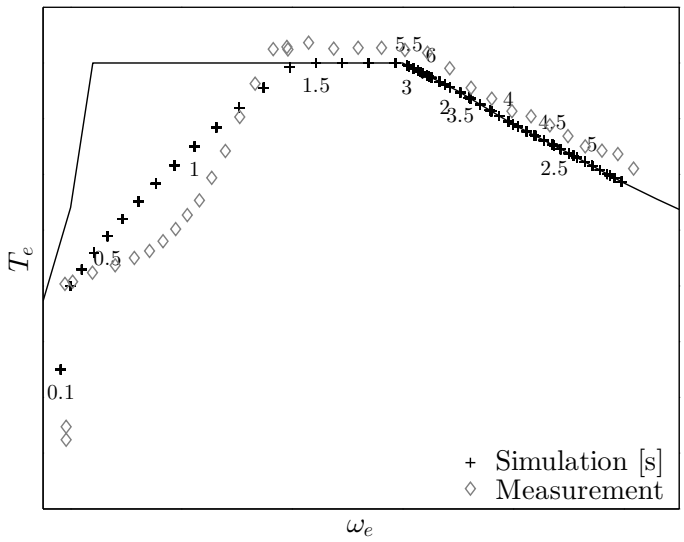

Figure 2.16: Comparison between simulation and measurements for full load operation with manually tuned map of permissible power.

power is of the order of 5 kW. At high values, significantly less turbolag is seen. The simulation is shown for the first 6 s. During this time, 2 gear upshifts are observed at 0.5 s and 4.9 s. The first upshift is observed at engine speed around 2000 rpm which is very unusual. This shift allows to operate at a higher engine torque and the direction of torque-speed trajectory thereafter provides higher acceleration and eventually leads to a higher terminal speed.

Next, the model was simulated with manually tuned map of permissible power dependent on the engine speed and the engine power, obtained based on practical knowledge and experience. This could eliminate the problem faced with the constant permissible power. However, when compared with the measurement from the test bench in the same simulation environment, the torque-speed trajectory quite differed. This comparison is shown in Fig. 2.16. In the measurements, the engine actually delivers slightly higher torque and power than theoretical limits used in the simulation. Nevertheless, it suggests that the map must be retuned to match the behavior of a real engine.

MODEL IV: Based on Map of Permissible Torque obtained through Regression

Subsequently, numerous experiments were conducted on the test bench in the same simulation environment with different initial gear n_g^{init} and vehicle speed v^{init}. The initial conditions of all the experiments are listed in Tab. 2.1.

One such experiment with $n_g^{\text{init}} = 1$ (n_g^1) and $v^{\text{init}} = 8\,\text{kmph}$ (v^8) has already been shown in Fig. 2.16. It is observed that the change in torque in consecutive time steps is strongly correlated with the permissible engine torque. This change is calculated for all the measurements in all the experiments and regression

Table 2.1: Initial vehicle speed for different initial gear in the experiments on the test bench. All speeds are in kmph. n_g^x refers to x gear number.

n_g^1	n_g^2	n_g^3	n_g^4	n_g^5	n_g^7
8	12	20	30	40	55
15	15	25	35	50	65
25	25	35	50	65	80
	35	50	65	80	100
			80	100	120

analysis based on MATLAB function `scatteredInterpolant` is used to create a function map

$$\Upsilon : (\omega_e, T_e) \rightarrow \Delta T. \tag{2.26}$$

Thus, given the engine speed and torque at a previous time step, the permissible torque at the current time step can be calculated using this model. Although some experiments have different initial gear, all of them can be used together to create a single map. By initialization at different gears, it has been possible to get data for a wide range of speed and torque. The map is actually independent of the initial gear number. This fact is further demonstrated in Fig. 2.17. At the point of intersection of torque-speed trajectory in different experiments, say (n_g^1, v^8) and (n_g^2, v^{25}), the torque gain in the next step is similar in both the cases.

The plot of function Υ thus obtained is shown in Fig. 2.18. The values in the naturally aspirated region are set to 0 which should ideally be as high as

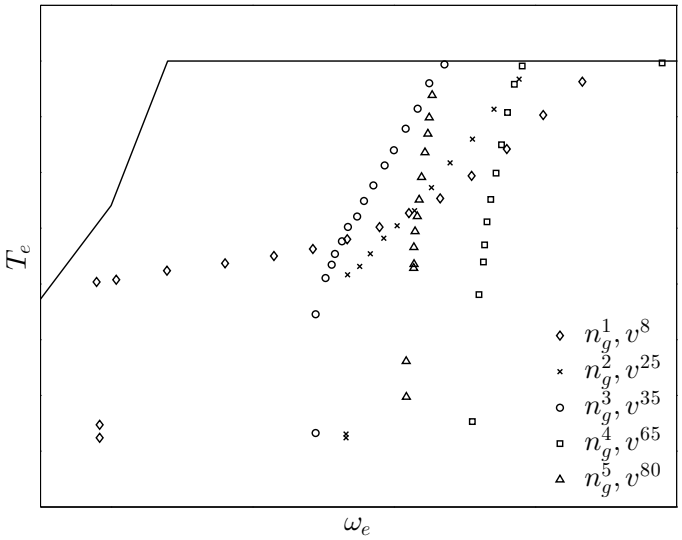

Figure 2.17: Experiments with different initial gear and speed showing the independence of Υ on gear number. Sampling time in these measurements is 0.1 s.

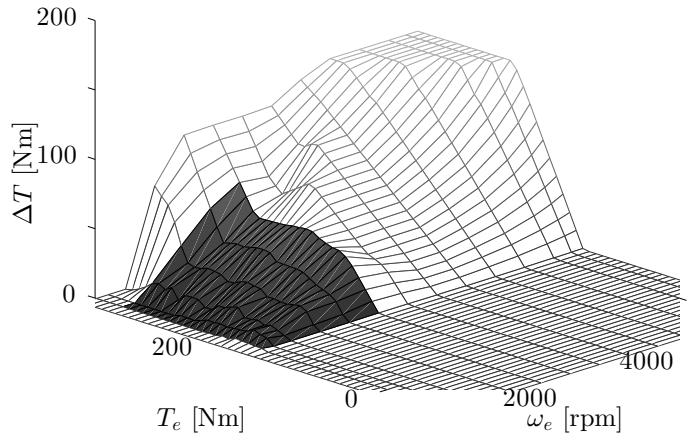

Figure 2.18: Map of permissible torque obtained through regression of the experimental data. Measurements were confined to the dark colored region, the remaining data has been extrapolated.

it is seen near the maximum power line of the engine because T_{na} is almost instantaneously achieved. This has been done to avoid interpolation errors at boundary but this fact has been considered in the vehicle model. Most of the measurements were made at low engine speeds, less than 3000 rpm where the effect of turbolag is the most prominent. At speeds greater than 3000 rpm, high ΔT has been manually specified and the engine torque is limited by $T_{e,\max}$ and not ΔT. As it is expected, the turbolag decreases with an increase in the engine speed. Therefore, the permissible engine torque increases.

This mapping yields a model with a new constraint defined by

$$\hat{T}_{e,\max}(t) = \min\left\{T_e(t-1) + \Delta T, T_{e,\max}(t)\right\}, \tag{2.27a}$$

$$\Delta T = \Upsilon(\omega_e(t-1), T_e(t-1)). \tag{2.27b}$$

The model has been validated against the measurements in the same simulation conditions and the results are in a very good agreement. The comparison for four such experiments is shown in Fig. 2.19. Now, the torque-speed trajectories for the case (n_g^1, v^8), unlike in Fig. 2.16, are very much alike. Also, the time taken to achieve the maximum engine torque is very similar. Except for the case when the engine speed exceeds 3000 rpm before reaching the maximum torque, the simulation and measurement results are very close. This is attributed to the fact that the number of measurements in that region are less, so the map could not be accurately trained. Nevertheless, this approach is seen to approximate the behavior of a turbocharged engine quite closely. Now, the turbolag is modeled using this approach in all the simulations in the next sections.

In summary, the limits on the engine torque, as a function of engine speed, can

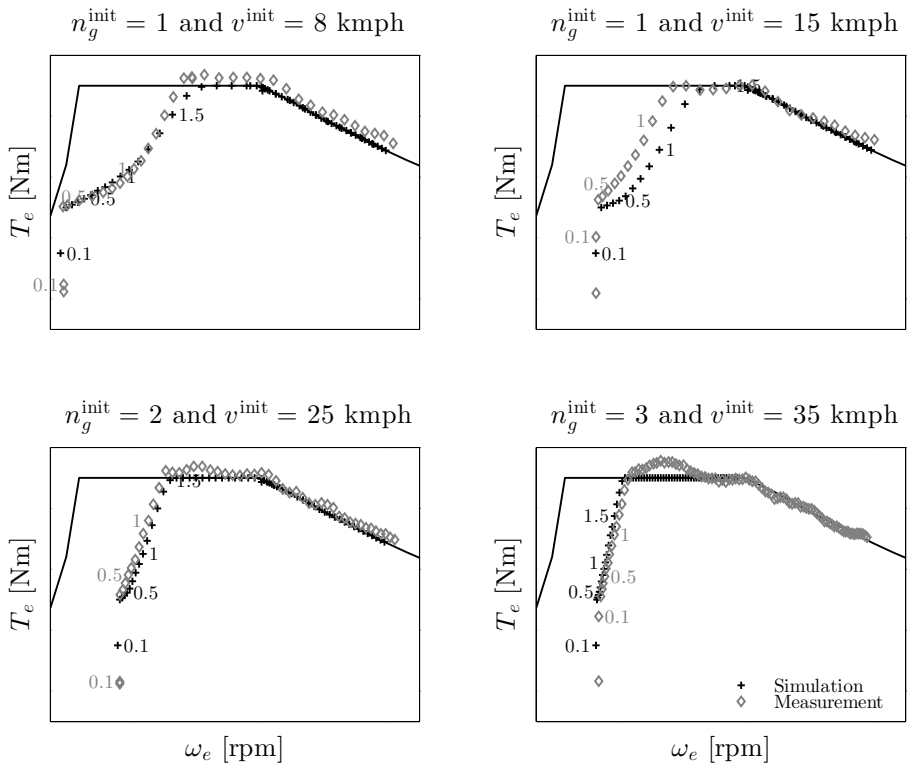

Figure 2.19: Validation of Model IV against experimental data. Time shown near the labels is in [s].

now be defined as

$$T_{e,\min}(\omega_e(t)) \leq T_e(t) \leq \hat{T}^{\text{M}_{\text{IV}}}_{e,\max}(\omega_e(t), \omega_e(t-1), T_e(t-1)). \tag{2.28}$$

2.5.3 Boost Mechanism

The power demand from the boost motor is used as an input in the control problem. The boost motor is directly coupled to the shaft of the turbocharger as shown in Fig. 2.20. This kind of setup is more suitable in application to hybrid electrical vehicles than mechanical turbocompounding because of the architectural advantages. ETC improves the transient response during acceleration and provides a better control alternative with an extra degree of freedom over its mechanical counterpart. However, building this assembly can be cost intensive.

The control input P_{tc} defines the electrical power demanded from the boost motor. Typically, the power of the order of 5 kW is sufficient to eliminate the major turbolag [39]. So, P_{tc} is constrained by

$$P_{tc,\min} \leq P_{tc} \leq P_{tc,\max}, \tag{2.29}$$

where $P_{tc,\min} = 0\,\text{kW}$ and $P_{tc,\max} = 5\,\text{kW}$. Depending upon the amount of electrical turbocharging, the limit on the engine torque imposed by the turbolag

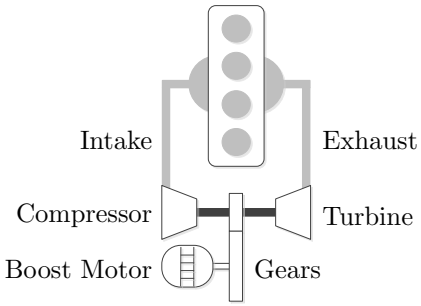

Figure 2.20: Turbocharger with motor/generator coupled to the shaft.

model can be increased. This mechanism for power assist is related to the energy required to accelerate the turbocharger by the dynamics equation

$$\Theta_{tc}\ \dot{\omega}_{tc} = \frac{P_t - P_c + \eta_{tc}\ P_{tc}}{\omega_{tc}}. \tag{2.30}$$

Here, P_t and P_c represent the power of the turbine and the compressor, respectively. Θ_{tc} is the moment of inertia of the turbocharger, η_{tc} the efficiency of the boost mechanism accounting for the energy losses and $\dot{\omega}_{tc}$ the angular acceleration of the shaft of the turbocharger. Under stationary conditions, P_t and P_c can be assumed to be equal in magnitude. Thus, the simplified dynamics of the shaft takes the form

$$\Theta_{tc}\ \dot{\omega}_{tc} = \eta_{tc}\ \frac{P_{tc}}{\omega_{tc}}. \tag{2.31}$$

To complete the description of the boost mechanism, the dynamics of turbocharger must be related to the torque constraint imposed by the turbolag. Recall Fig. 2.11 where the turbocharger speed was calculated for all the operating points. It is now used to calculate the turbocharger speed at an operating point defined by $(\hat{T}_{e,\max}(t), \omega_e(t))$ at any time instant t. This would be the speed of the turbocharger if the constraint (2.27) is active. In other words, this speed of the turbocharger is achievable without any need of electrical turbocharging. Now, the differential equation (2.31) can be integrated over a sampling time for a given P_{tc} to calculate the new turbocharger speed:

$$\omega_{tc}^{\mathrm{T_s}}(t) = \sqrt{\left(\omega_{tc}^{0}(t)\right)^2 + 2\ \eta_{tc}\ \frac{P_{tc}\ T_s}{\Theta_{tc}}}, \tag{2.32}$$

where the initial condition given by

$$\omega_{tc}^{0}(t) = \omega_{tc}\Big|_{(\hat{T}_{e,\max}(t), \omega_e(t))}\ . \tag{2.33}$$

The new turbocharger speed $\omega_{tc}^{\mathrm{T_s}}(t)$ defines a new limit on maximum engine torque $\tilde{T}_{e,\max}$ using the map Ω given by (2.22b). This mechanism is further described in Fig. 2.21.

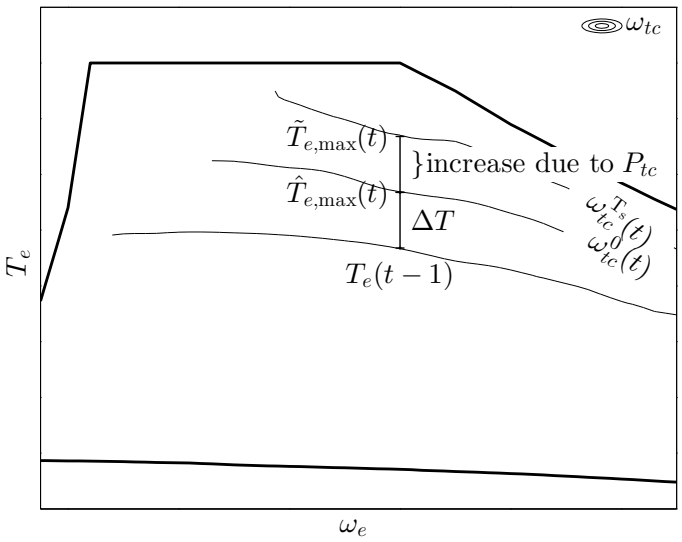

Figure 2.21: Mechanism for power boost.

2.6 Battery

The causality relation for the battery is shown in Fig. 2.22. The sum of the power from the two motors and the auxiliary power is the net power input, also called the terminal power of the battery P_b. The output is the battery charge Q. The terminal current I_b of the battery is defined by

$$I_b = \frac{P_b}{U_b}, \tag{2.34}$$

$$P_b = P_m + P_{tc} + P_{\text{aux}}, \tag{2.35}$$

where U_b is the terminal voltage. It can be expressed as a function of open circuit voltage U_{oc}, terminal power P_b and internal resistance of the battery R_b

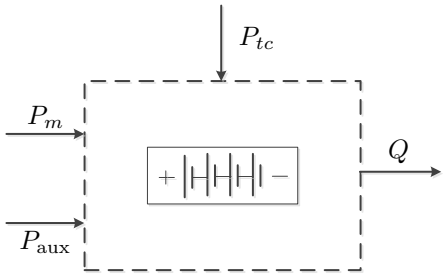

Figure 2.22: Quasistatic model of a battery.

as

$$U_b = \frac{U_{oc}}{2} + \sqrt{\frac{U_{oc}^2}{4} - P_b \; R_b}. \tag{2.36}$$

The terminal power is a quadratic function of the terminal voltage. By calculating the derivative of P_b with respect to U_b, the limits on the terminal power can be derived:

$$P_{b,\min} \leq P_b \leq P_{b,\max}. \tag{2.37}$$

The state of charge (SoC) of the battery ξ, which is also one of the states in the control problem, is the ratio of charge Q and charge capacity Q_0,

$$\xi = \frac{Q}{Q_0}. \tag{2.38}$$

The reference model uses a lithium-ion battery with a charge capacity 2.4 Ah. The SoC must lie in a SoC window defined by the quantity of charge a battery can store while charging and discharging. Therefore,

$$\xi_{\min} \leq \xi \leq \xi_{\max}. \tag{2.39}$$

The variation of the SoC depends on the terminal current as follows

$$\dot{\xi} = -\frac{\eta_{cb} \; I_b}{Q_0}, \tag{2.40}$$

where η_{cb} is the coulombic efficiency. $\eta_{cb} = 1$ is used in the calculations. An estimation of the terminal voltage and the internal resistance as a function of ξ can be done online [23]. Here, it is has been used in form of maps. Finally, substitution of equations (2.34)-(2.36) into (2.40) yields the change in SoC.

Chapter 3

Supervisory Control

The task of a supervisory controller is to decide how the energy requirements should be distributed optimally between different available paths like ICE, traction motor and boost motor while satisfying the driveability constraints. The performance in this control problem is optimized independently with respect to two objectives: fuel consumption and acceleration performance, by calculating 3 optimal control inputs: torque split between engine and traction motor, power of boost motor and gear number. In the latter case, while optimizing the acceleration performance, the engine torque split variable becomes redundant (see Sec. 3.5) and only 2 inputs are required.

Numerical optimization method like Dynamic Programming (DP) forms a natural choice as a solution method for this control problem but it requires large computation time and it is dependent on a driving cycle which is not known during a real-time implementation. Nevertheless, it provides a benchmark for the comparison with other control strategies. Other very well established solution methods include model predictive control with DP(MPC-DP) [2, 6, 13, 35], stochastic DP (S-DP) [28, 38], Pontryagin's Minimum Principle (PMP) [12, 31], ECMS & its variants adaptive ECMS (A-ECMS) [40], telemetry ECMS (T-ECMS)[47], fuzzy-tuned ECMS (F-ECMS) [61] and Convex Optimization with DP (Cvx-DP) [41]. All of which can be implemented online with a simple model achieving near optimal results. Presence of multiple states in this system increases the computational effort in DP because of the so called *curse of dimensionality*. At the same time, it can also be cumbersome to tune the co-states in PMP and ECMS in the presence of new state constraints or new cost terms [48]. Infact, due to same reason, the available literature on PMP is mostly limited to one state or doesn't account for an additional cost in the hamiltonian.

In this chapter, a control strategy for energy management based on Dynamic Programming has been derived for an electrically assisted turbocharged parallel HEV. First, the procedure to solve optimal control problem with DP is introduced. Then, the problems for two different objectives, fuel economy in Sec. 3.4 and acceleration performance in Sec. 3.5, are defined. In the last section of this chapter, the complexity involved in implementing PMP with this system is discussed.

3.1 Optimal Control

A standard optimal control problem with a finite horizon N can be represented by the set of equations (3.1). The dynamic system has n states, m inputs and p disturbances.

Objective:

$$\min \left\{ g_N(x_N) + \sum_{k=1}^{N-1} g_k(x_k, u_k, w_k) \right\} \tag{3.1a}$$

Constraints:

$$x_{k+1} = f_k(x_k, u_k, w_k), \tag{3.1b}$$

$$x_k \in X_k \subseteq \mathbb{R}^n, \tag{3.1c}$$

$$u_k \in U_k \subseteq \mathbb{R}^m, \tag{3.1d}$$

$$w_k \in W_k \subseteq \mathbb{R}^p, \tag{3.1e}$$

$$x_0 = X_0, \tag{3.1f}$$

$$\forall\, k \in 0, 1, 2 \ldots N.$$

Here x_k, u_k and w_k represent the state, the control input and the disturbance vector, respectively, at discrete time index k. g_N is the terminal cost dependent on the terminal state x_N. g_k is the state cost defining the cost incurred in going from state x_k to x_{k+1}. Dynamics of the system is defined by (3.1b). x_k, u_k and w_k are constrained to lie in the sets X_k, U_k and W_k, respectively, where U_k may be a function of X_k, and W_k of X_k and U_k . The goal is to find an optimal set of control inputs $u := [u_0, u_1, ...u_{N-1}]^T$ which minimizes the cost (3.1a). In the control problem considered here, w_k is deterministic, otherwise an expected value of sum of the terminal and the stage costs must be used.

3.2 Dynamic Programming

One of the ways to solve (3.1) is by dynamic programming [4] which uses principle of optimality to break this problem into N subproblems. It can be summarized in two steps.

Initialization: Cost is defined for each terminal state.

$$J_N(x_N) = g_N(x_N),\ \forall x_N \in X_N \tag{3.2a}$$

Recursion: Optimal u_k^* and cost-to-go $J_k(x_k)$ are calculated for all x_k at each recursion step k proceeding backward in time.

$$J_k(x_k) = \min_{u_k \in U_k} \{ g_k(x_k, u_k, w_k) + J_{k+1}\left(f_k(x_k, u_k, w_k)\right) \} \tag{3.2b}$$

Table 3.1: Different scenarios for comparing vehicular performance.

	Case I	Case II
ICE	Turbocharged	Turbocharged
$P_{e,\max}$	155 kW	155 kW
$P_{m,\max}$	20 kW	20 kW
$P_{tc,\max}$	5 kW	0 kW
$P_{el,\max}$	20 kW	20 kW
$E_{b,0}$	1.2 kWh	1.2 kWh

Thus, $u_k^* := \mu_k^*(x_k)$ is the argument that minimizes (3.2b). $\mu^* := [\mu_1^*, \mu_2^* \dots \mu_{N-1}^*]$, which minimizes the optimal cost $J_0(x_0)$, is referred to as the optimal control policy. DP necessitates gridding of states and inputs. Therefore, the states dynamics must also be discretized and an interpolation between different gridded points is required. The grid size should be defined such that the optimal solution is not affected by numerical errors. Moreover, the cost for the non-reachable states should also be defined appropriately to avoid further errors due to interpolation [17].

3.3 Simulation Environment

The reference P1 HEV described in Chap. 2 is used throughout this chapter. To analyze the effectiveness of an e-boost mechanism in an HEV, control strategies in two different scenarios will be compared, see Tab. 3.1. Case II represents an HEV without assisted turbocharger i.e. the boost motor is always switched-off. So, the traction motor is the sole source of electrical energy in the system. In the other case, the traction motor and the boost motor both can provide electrical power, but the maximum electrical power $P_{el,\max}$ is same in both the cases (also see (3.3j)). With an additional degree of freedom, the total electrical power is optimally distributed between the two motors in Case I. All the other vehicle parameters are same in both the cases.

Sampling time of 0.1 s is used wherever not specified. The control problem was solved using MATLAB based dpm-function [52]. All the simulations were carried out on 2.7 GHz i7 processor. In the context of energy management in HEVs, the approach to solve the problem by DP has been adapted from [22].

3.4 Fuel Consumption

The fuel consumption of an engine depends on the selection of operating points in a driving cycle. The task of the controller is to optimally select these set points that attain a charge-sustaining operation while satisfying all model and driveability constraints. In addition to the constraints derived in the Chap. 2, the total electrical power available at any time is also limited. This helps to study the circumstances under which either of the motors should be used and also the distribution of the total electrical power between the two.

To model turbolag, ω_e and T_e must be included as states. So, the corresponding control problem can be formulated with 3 states: SoC, engine speed and engine torque defined by $x := [\xi, \omega_e, T_e]$, 3 inputs: engine torque split, gear number and power of the boost motor defined by $u := [\zeta, n_g, P_{tc}]$ and 3 deterministic disturbances: speed of the vehicle, acceleration of the vehicle and driving slope defined by $w := [v, a, \alpha]$ as follows:

Objective:

$$\min \left\{ \phi(\xi(T)) + \int_0^T \dot{m}_f dt \right\} \tag{3.3a}$$

Constraints:

$$\xi_{k+1} = \xi_k - \frac{\eta_c \; I_b(x_k, u_k, w_k)}{Q_0} \; T_s, \tag{3.3b}$$

$$T_{e,k+1} = (1 - \zeta_k) \; T_{gb,k}(x_k, u_k, w_k), \tag{3.3c}$$

$$\xi_{\min} \leq \xi_k \leq \xi_{\max}, \tag{3.3d}$$

$$P_{b,\min}(\xi_k) \leq P_{b,k} \leq P_{b,\max}(\xi_k), \tag{3.3e}$$

$$\omega_{e,\min} \leq \omega_{e,k} \leq \omega_{e,\max}, \tag{3.3f}$$

$$T_{e,\min}(\omega_{e,k}) \leq T_{e,k} \leq \hat{T}_{e,\max}(\omega_{e,k}, \omega_{e,k-1}, T_{e,k-1}), \tag{3.3g}$$

$$\omega_{m,\min} \leq \omega_{m,k} \leq \omega_{m,\max}, \tag{3.3h}$$

$$T_{m,\min}(\omega_{m,k}) \leq T_{m,k} \leq T_{m,\max}(\omega_{m,k}), \tag{3.3i}$$

$$P_{m,k} + P_{tc,k} \leq P_{el,\max}, \tag{3.3j}$$

$$\zeta_{\min} \leq \zeta_k \leq \zeta_{\max}, \tag{3.3k}$$

$$n_{g,\min} \leq n_{g,k} \leq n_{g,\max}, \tag{3.3l}$$

$$P_{tc,\min} \leq P_{tc,k} \leq P_{tc,\max}, \tag{3.3m}$$

$$\xi_0 = \xi^0, \; \omega_{e,0} = \omega_e^0, \; T_{e,0} = T_e^0, \tag{3.3n}$$

$$\forall \; k \in 0, 1, 2 \ldots N.$$

The function ϕ in (3.3) penalizes the end state-of-charge so that a charge-sustaining operation can be attained. It is a linear function given by

$$\phi(\xi(T)) = \mu_{cs}\ (\xi(T) - \xi^0), \tag{3.4}$$

where μ_{cs} is a constant [22]. The state dynamics equations (3.3b) and (3.3c) can be written explicitly in terms of model states and inputs by substituting the model equations derived in Chap. 2. The constraint (3.3j) limits the total available electrical power. The initial value of the state-of-charge $\xi^0 = 0.6$ has been used. The initial engine speed torque ω_e^0, T_e^0 can be calculated from the driving cycle. T represents the final time in the driving cycle.

3.4.1 Results in NEDC and WLTC

An initial investigation on fuel consumption of the reference vehicle is done in common driving cycles like New European Driving Cycle (NEDC) and Worldwide harmonized Light vehicles Test Cycle (WLTC). The results have been recorded in Tab. 3.2. The boost motor was inactive in these simulations, meaning there are only 2 control inputs. A comparison is shown with an ideal model of the reference engine i.e. the same turbocharged engine but without any turbolag. It is clear that the turbolag doesn't affect the fuel consumption to a great extent in these cycles which also rules out potential benefits of employing another electrical machine in the form of boost motor.

Table 3.2: Difference in fuel consumption [$^{l}/_{100\text{km}}$] between a turbocharged engine with (lag) and without turbolag (nolag) in NEDC and WLTC. The final SoC is same as the initial SoC in all the simulations.

	$\int \dot{m}_{f,\text{lag}} dt - \int \dot{m}_{f,\text{nolag}} dt$
NEDC	0.002
WLTC	0.008

The operating points in NEDC and WLTC are illustrated on the engine map in the Fig. 3.1. The plots show that the torque demands in these cycles are too low and most of the operating points lie in the naturally aspirated region of the engine map. Therefore, a new driving cycle is considered in the next section which has more rapid acceleration phases and thus higher torque demands.

3.4.2 Selection of a Suitable Driving Cycle

Many driving cycles (DC) with different constant acceleration and deceleration phases were analyzed. These are shown in Fig. 3.2. Again, the fuel consumption was optimized by switching off the boost motor. All the cycles have same maximum speed and deceleration rate. Acceleration in DC I is the highest and it is the least in DC III. It is observed that the difference in fuel consumption between an engine with and without turbolag increases monotonously with an increase in magnitude of the acceleration, see Tab. 3.3. The higher the acceleration, the higher is the torque demand. This results in more number of

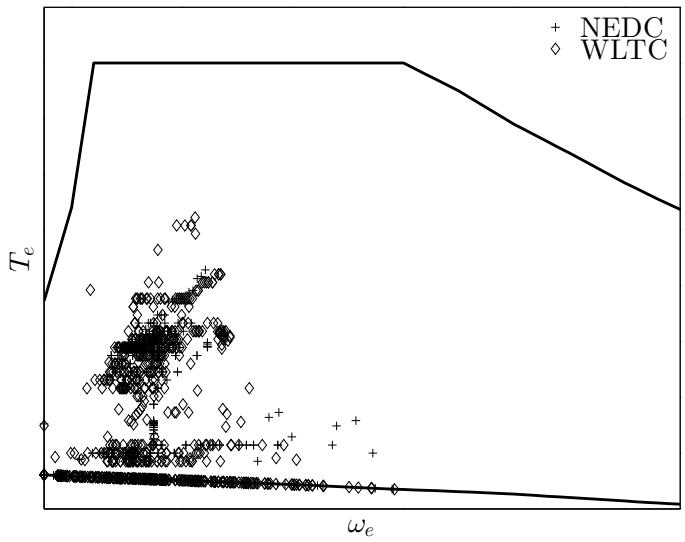

Figure 3.1: Engine operating points in NEDC and WLTC. Very few points lie in the turbocharged region of the map.

operating points in the turbocharged region (dome shape) of the engine map and the effect of turbolag on fuel consumption comes into picture. These points are shown in Fig. 3.3. In DC III, almost all the points lie below 225 Nm, so the effect of turbolag is still not visible in the fuel consumption. Consequently, a boost motor is not at all required in this kind of a driving cycle. As the engine torque rises in DC I and DC II, the fuel consumption increases in the presence of turbolag. In comparison to NEDC and WLTC, average engine torque in these cases is much higher. Still the fraction of points in the turbocharged region of the engine map in DC I is low. If this fraction can be increased, even a higher difference in fuel consumption will be seen.

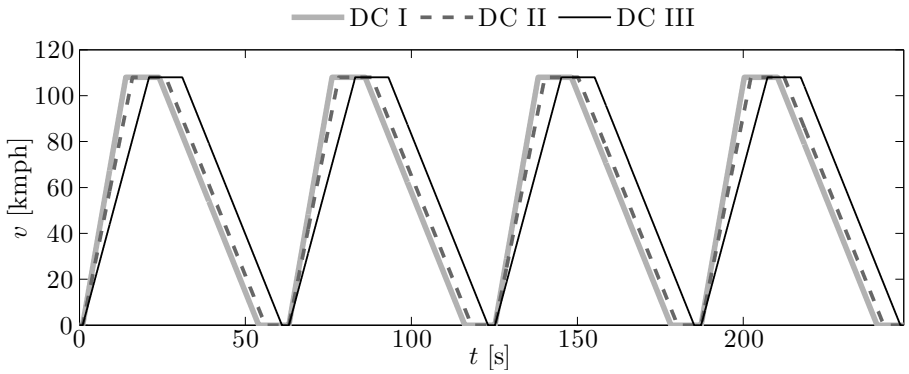

Figure 3.2: Different driving cycles with varying acceleration demands (repeated 4 times). Driving cycle I has the maximum acceleration & driving cycle III the least.

Table 3.3: Difference in fuel consumption [$^{l}/_{100\text{km}}$] in DC I, II and III between a turbocharged engine with (lag) and without turbolag (nolag). The difference between these increases with an increase in maximum torque demand.

	$\int \dot{m}_{f,\text{lag}} dt - \int \dot{m}_{f,\text{nolag}} dt$
DC I	0.05
DC II	0.01
DC III	0.00

3.4.3 Results in a Fast Driving Cycle

On the basis of these findings, a real-life driving situation is considered, see Fig. 3.4a. This driving cycle is simulated by running the HEV model, switching off the boost motor, at full throttle in the 5^{th} gear starting at 50 kmph. Under these circumstances, the load demand is so high that, without an electrical boost, both the engine and the traction motor must be used continuously to meet the power demands. Thus, it is impossible to have a charge-sustaining strategy without a boost motor.

A performance analysis has been done for 2 scenarios described in Sec. 3.3. Because a charge-sustaining strategy is not possible in Case II, at first, a comparison between the two cases with same end state-of-charge $\xi(T)$ $(< \xi^0)$ is shown in the Fig. 3.4. The gear number is fixed at 5. The fuel consumption in Case I (with e-boost) is slightly less than in Case II. In the presence of e-boost, the engine torque can be built up very fast, otherwise the operation strategy for the engine torque is almost the same as in Case II. Whenever the boost motor is switched on, less amount of power is available for the traction motor. Although a slight reduction in fuel consumption is observed in this process, the boost

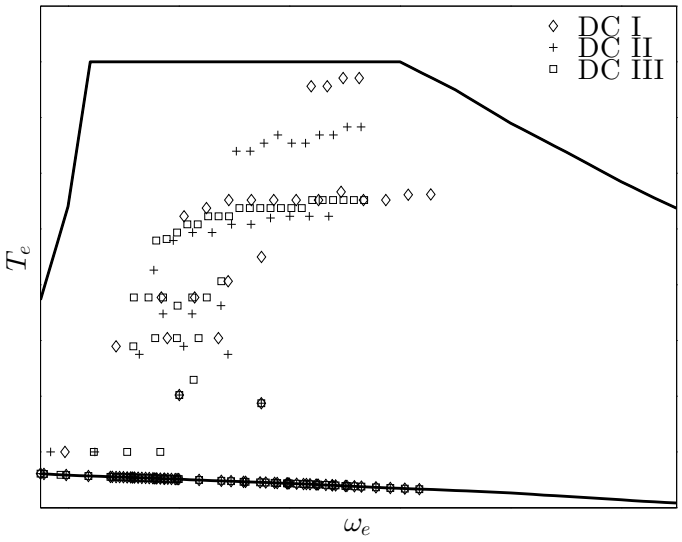

Figure 3.3: Engine operating points in DC I, II and III.

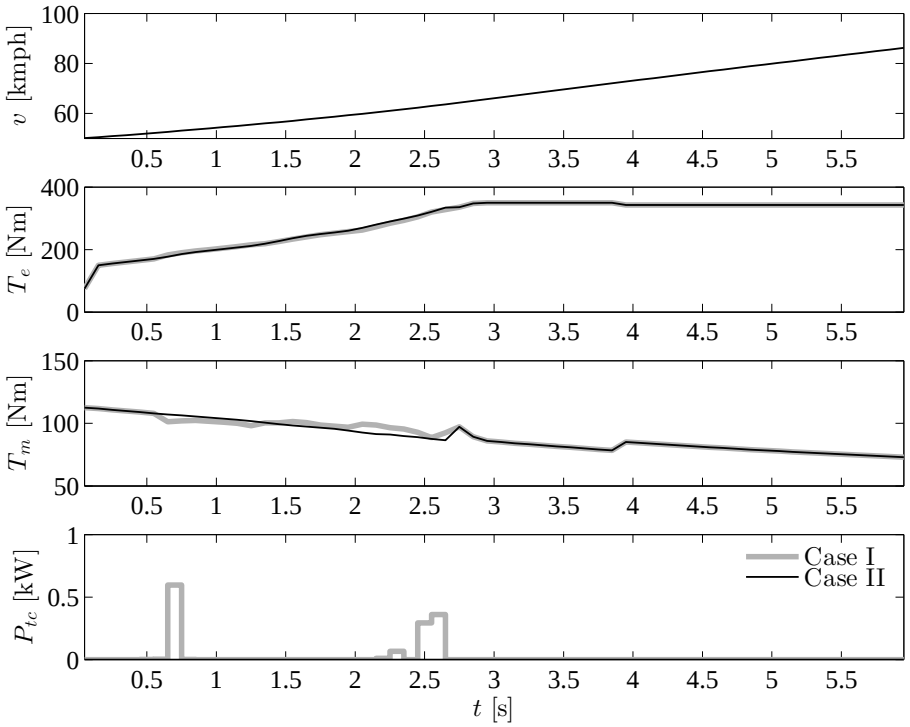

Figure 3.4: Comparison between Case I (HEV with e-boost) and Case II (HEV without e-boost) while driving at full throttle in 5^{th} gear. $\xi(T)$ is same in both the simulations.

motor provides power intermittently which may not be practically realizable. Overall, the changes in the operation strategy are not clearly visible.

In Case II, there is not much freedom on the final SoC as the power demand is very high and both the engine and the traction motor operate at their maximum potential nearly most of the times. If the terminal SoC in Case I is constrained at a higher level, the boost motor works steadily for a longer duration. The engine torque can be built up even faster and this extra torque is utilized to recharge the battery. This charging comes at an expense of fuel consumption. By forcing the boost motor to work for a longer time, the engine operates at inefficient set points which increases the fuel consumption. These results, classified as Case $\mathrm{I_b}$, are shown in Fig. 3.5 in comparison with Case I. The engine torque between $0.5\,\mathrm{s} - 2.5\,\mathrm{s}$ is much higher in Case $\mathrm{I_b}$, correspondingly the motor torque is much lower. Therefore, with the help of electrical boost, the battery can be forcefully recharged when torque demands are too high and there is not sufficient time to obtain a strategy charge-sustaining otherwise.

The increase in fuel consumption in Case $\mathrm{I_b}$ is visible from the operating points in Fig. 3.6. On an average, the efficiency of operating points in Case I is higher. This indicates that the forced recharging of the battery in Case $\mathrm{I_b}$ is a fuel inefficient process.

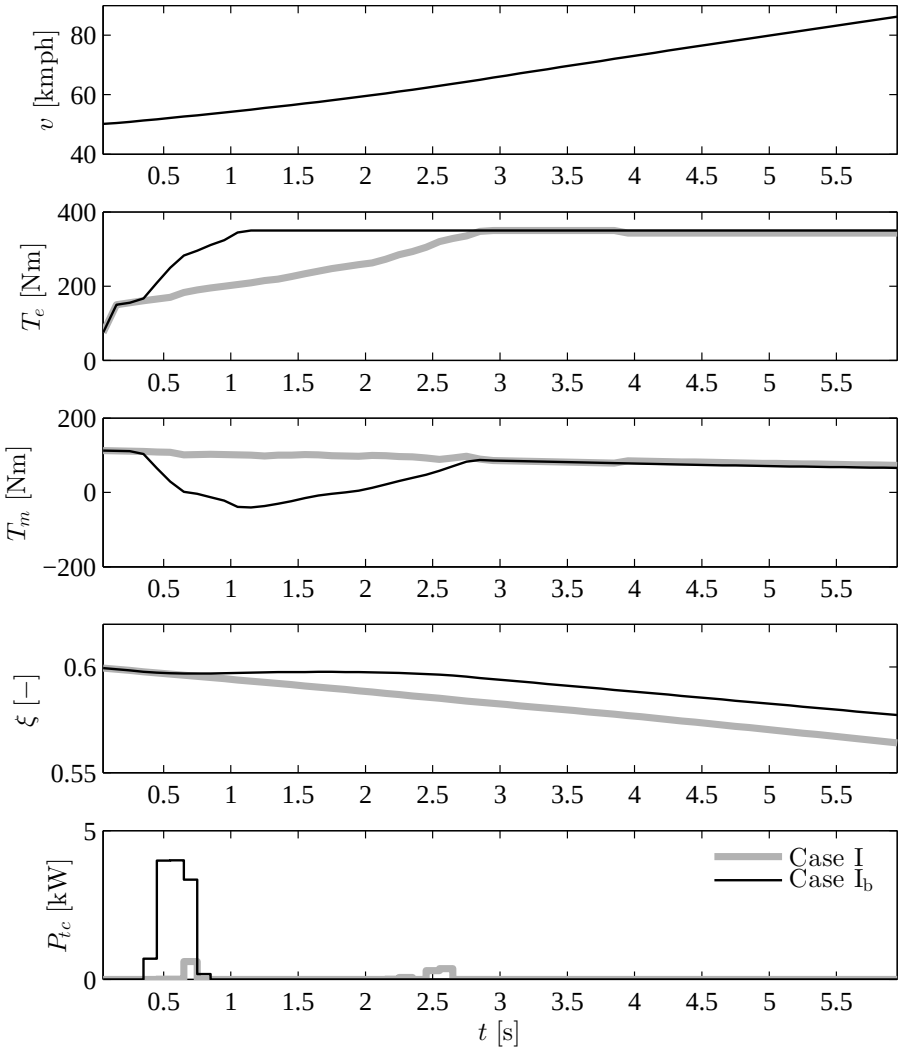

Figure 3.5: Comparison between Case I (HEV with e-boost) and Case I_b (HEV with e-boost and forceful recharging) while driving at full throttle in 5^{th} gear. Case I_b uses boost motor steadily to attain a higher end SoC but sacrifices on fuel consumption.

The numerical results from Fig. 3.4 and 3.5 are listed in Tab. 3.4. Case I shows only theoretical benefits over Case II. With the same terminal SoC, Case I uses boost motor intermittently to slightly reduce the fuel consumption. In this type of a cycle, the possibility of recharging doesn't exit in Case II because the motor must always operate in traction mode. The boost motor is useful if the battery needs to be recharged (Case I_b) but an additional amount of fuel must be spent. For approximately 1.3% increase in SoC (over Case I) of 1.2 kWh battery, 3 g of extra fuel is burnt in every 110 m (length of the driving cycle). This gives fuel to electrical energy equivalence factor of 2.3.

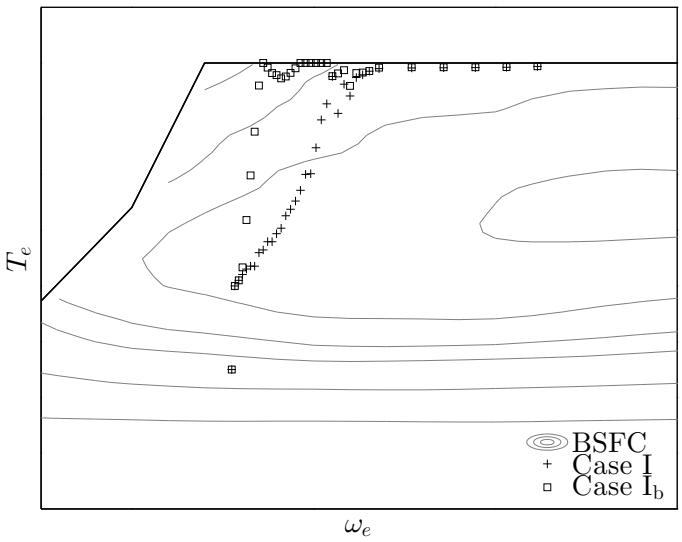

Figure 3.6: Engine Operating points in Case I (HEV with e-boost) and Case I$_b$ (HEV with e-boost and forceful recharging) while driving at full throttle in 5^{th} gear. Case I$_b$ shows significantly less turbolag as the boost motor is used during build up.

New Fast Driving Cycle

Next, a new fast driving cycle (NFDC) is designed, as shown in Fig. 3.7, in which a charge sustaining solution is possible even without a boost motor. It resembles a driving pattern in mild/heavy traffic conditions on highways. An important feature of this cycle is the frequent change in power required to drive the vehicle. Also, the maximum acceleration in NFDC is $2.4\,\mathrm{m/s^2}$, much higher than in NEDC and WLTC. Higher torque demands, in this case, shifts many operating points in the turbocharged region (Fig. 3.8) and the effect of turbolag on the fuel consumption is expected.

A preliminary comparison between the 2 model cases defined in Tab. 3.1 was done by using a heuristics-based gear strategy which is same in both the cases. The resulting engine torque, traction motor torque and the power of the boost motor are shown in Fig. 3.9. The main difference in the strategies arise in the

Table 3.4: Comparison of normalized fuel consumption $[-]$ in Case I and Case I$_b$ with respect to Case II while driving at full throttle in 5^{th} gear.

	Case I	Case I$_b$	Case II
Fuel Consumption	0.998	1.126	1.000
$\xi(T)$	0.564	0.577	0.564
ξ^0	0.6	0.6	0.6

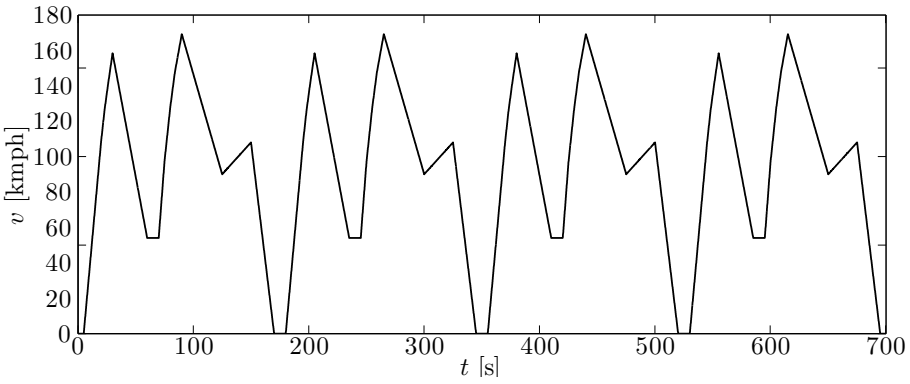

Figure 3.7: NFDC: An example of a driving cycle with very high acceleration requirements (repeated 4 times).

events of high gradients in torque demands. For instance between $66 - 70\,\mathrm{s}$, in Case I, the boost motor assists the engine in overcoming turbolag, while in Case II, the engine starts some time in advance to reduce the effect of turbolag. To compensate for a short running time and still achieve a charge-sustaining strategy, the engine in Case I produces higher torque in the later part of the driving cycle. At times when the boost motor is used, the capacity of the traction motor is reduced because the total electrical power is fixed. It is observed that the fuel consumption in Case I is lower than in Case II, see Tab. 3.5. Even though the boost motor is used for a very short duration, it reduces the fuel consumption. Again, the boost motor is used intermittently, initially for $0.3\,\mathrm{s}$ and later for $0.1\,\mathrm{s}$.

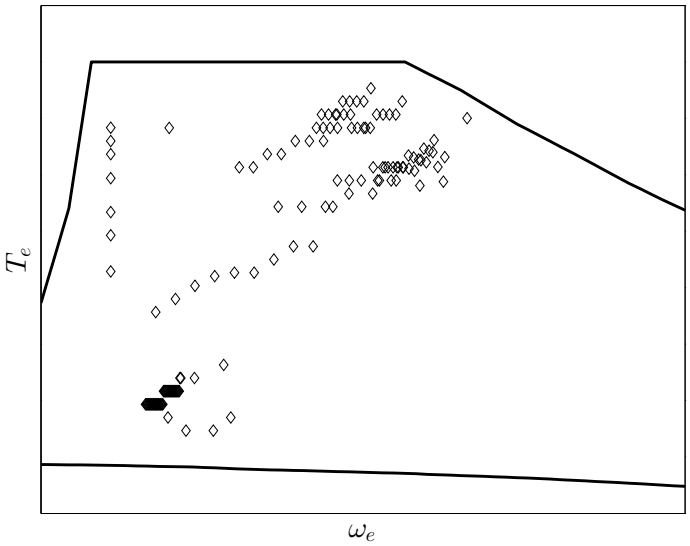

Figure 3.8: Engine operating points in new fast driving cycle (Fig. 3.7). Many points in the turbocharged region can be seen.

Table 3.5: Comparison of normalized fuel consumption [−] in Case I with respect to Case II in NFDC with heuristics-based gear strategy.

	Case I	Case II
Fuel Consumption	0.993	1.000
$\xi(T) - \xi^0$	-0.001	-0.003

3.4.4 Conclusion

Overall, using a boost motor in an HEV does not show major improvement in fuel economy. However, the results suggest that it could be beneficial in special circumstances to recharge the battery when it is not possible to make the strategy charge-sustaining otherwise. Here, the boost mechanism has been used only in the motor mode. Using it in the generator mode could potentially save some fuel but it could not be verified with these set of models and it needs more research and time.

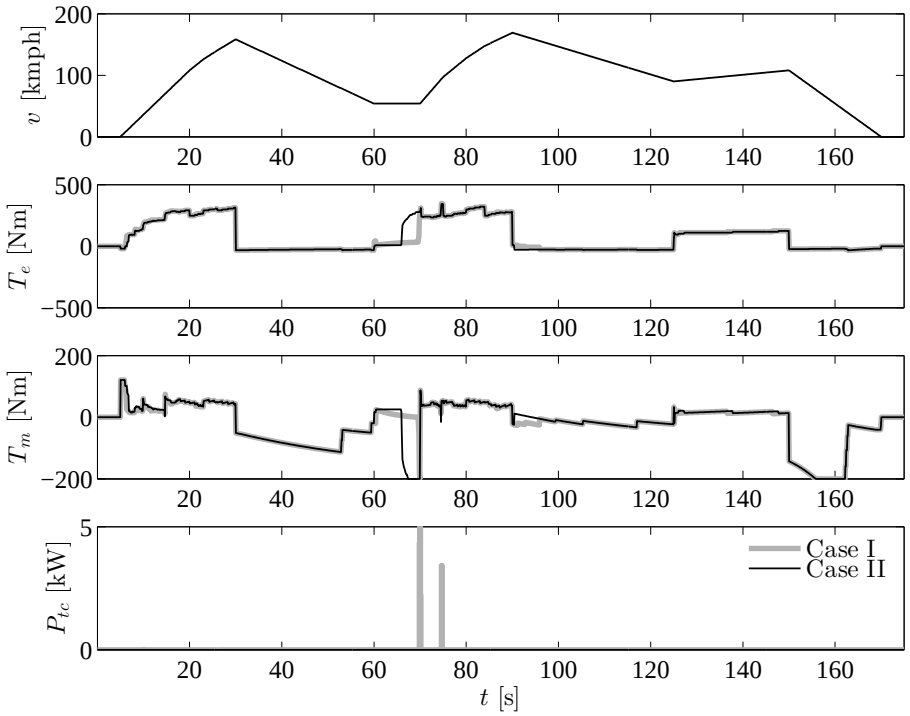

Figure 3.9: Simulations for Case I and Case II in NFDC with heuristics-based gear strategy.

3.5 Driving Performance

3.5.1 Measures of Driving Performance

Optimal fuel consumption without consideration to driveability may not offer good driving experience. There are a number of ways to quantify driving performance/comfort. Some of them are listed below:

- *Constraint for Smooth Drive:* Ensures that engine speed is a monotonic function of vehicle speed and power required at wheels. It requires engine speed as another state [59].

- *Penalty on Jerk:* Limits rapid changes in acceleration. It also requires engine speed as another state [62].

- *Penalty on ICE On/Off:* Reduces frequent engine on/offs. It requires engine on/off condition as a state [42].

- *Penalty on Gear Shift:* Restricts frequent gear shifts. It requires gear as a state and a penalty is imposed on change in subsequent gear positions [37, 42].

- *Heuristic Gear Strategy:* Uses a predefined gear strategy for smooth gear shifting [45].

- *Penalty on Torque Change:* Limits rapid changes in the torque that engine delivers. It affects the gear shift strategy indirectly and requires engine torque as one of the states in the control problem.

- *Penalty on Power Reserve:* Keeps power in reserve which could be required at any time but is not required on the driving cycle for which the control strategy is designed. It can be defined based on the difference between the power delivered and maximum that can be delivered at any time instant.

- *Fast Acceleration:* Accelerates the vehicle as fast as possible. Apart from more states in the form of vehicle speed and gear, the control problem must also be modified for this measure.

Several other ways to evaluate the driving performance can be found in [58]. All the above methods, except for the last one, can be implemented in the same way as the fuel optimal control problem by adding additional costs or constraints in DP. To optimize the acceleration response, the control problem needs to be restructured in the form of minimal time problem [33]. In the context of an HEV with electrically assisted turbocharger, this approach is discussed here.

3.5.2 Acceleration Performance

The objective in this case is to accelerate the vehicle as fast as possible and minimize the time to achieve a desired speed v_{des}, say 100 kmph. This usually takes under 10 s for the reference vehicle and there is just not enough time to make the strategy charge-sustaining. It is more interesting to analyze the power split between the two motors under the constraint of fixed total available electrical power. Intuitively, under this constraint, ICE must be used at each time instant delivering as much torque as possible. Therefore, apart from the gear strategy,

the the controller should only decide when and how much power should each of the motors provide.

This problem can be formulated with 3 states $x := [v, T_e, n_g]$ and 4 inputs $u := [\zeta, n_g, P_{tc}, a]$. Now, ξ can be eliminated from the state vector because SoC is no longer under consideration. $\omega_{e,k-1}$, which was one of the sates in 3.3, can be estimated from the states v and n_g. Since, no driving cycle is required in this case, there is no disturbance vector w. Instead, a has been included in the input vector and α is taken as zero.

Objective:

$$\min \ T \tag{3.5a}$$

Constraints:

$$v_{k+1} = v_k + a_k T_s, \tag{3.5b}$$

$$T_{e,k+1} = (1 - \zeta_k)\ T_{gb,k}(x_k, u_k), \tag{3.5c}$$

constraints (3.3f)-(3.3m),

$$a_k \leq a_{\max}, \tag{3.5d}$$

$$v_0 = v^0,\ n_{g,0} = n_g^0,\ T_{e,0} = T_e^0,\ v_N = v_{\text{des}}, \tag{3.5e}$$

$$\forall\ k \in 0, 1, 2 \ldots N.$$

This is a type of minimal time problem [4] where the end time is free and must be calculated by solving the optimal control problem. The cost is required only for the final time T. Therefore,

$$g_k(x_k, u_k) = 0,\ \forall\ k < N. \tag{3.6}$$

Note that v is required as one of the states here, unlike while optimizing fuel consumption where it is considered as a disturbance from the driving cycle. Inputs ζ and a are essentially redundant because the quantities of interest are only the gear number and the split between total available electrical power. By including these variables in the control vector, it is possible to solve the problem in the same manner as in Section 3.4. But at the same time, it unnecessarily increases the computational burden.

With a slight manipulation, the set of equations (3.5) can be converted into a fixed time optimal control problem. Instead of minimizing the final time T, the final vehicle speed v_N can be maximized for a fixed time $T := NT_s$. Now, the optimal trajectory v_k^* can be used to calculate the optimal time N^* such that $v_{N^*} = v_{\text{des}}$. So, the objective function (3.5a) can be redefined as:

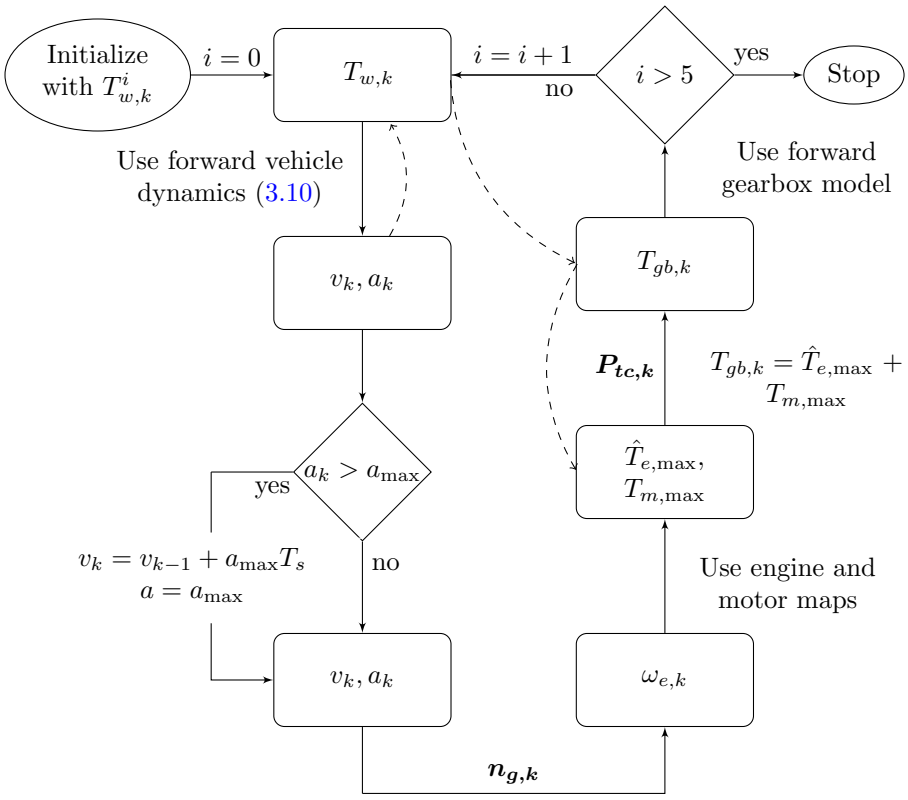

Figure 3.10: Flowchart for the iterative procedure to reduce number of control inputs. The symbols in bold represent the control inputs. Dashed lines in the figure correspond to the old procedure with 4 control inputs (3.5).

Objective:

$$\min \quad -v_N \tag{3.7}$$

As said before, the drawback of this approach lies in the number of required inputs which unnecessarily increases the time complexity with DP because a is not an independent variable. In fact, both a and ζ can be eliminated to make the algorithm efficient by finding a right combination of a and T_{gb} which maximizes the performance. Equivalently, this can be done by delivering as much torque as possible, the limit being defined by either the maximum acceleration $a_{\max}$ or the sum of the maximum engine torque $\hat{T}_{e,\max}$ and the maximum motor torque $T_{m,\max}$. This maximum limit on torques depends on vehicle speed which in turn depends on vehicle acceleration. Because of this circular relationship, an iterative procedure is required to get rid of the redundant variables. This method uses both forward and backward models and is illustrated in Fig. 3.10.

While solving with the new approach, $T_{w,k}$ is initialized with a small value, corresponding to maximum torque at idling speed. Then, the forward model

for the vehicle dynamics

$$T_w = r_w \left((m_v + m_r)\ a + \frac{1}{2}\ \rho_{\text{air}}\ A_{\text{fr}}\ C_d\ v^2 + m_v\ C_r\ g \right) \tag{3.8}$$

gives a unique solution for v_k and $a_k (> 0)$ using $a_k\ T_s = v_k - v_{k-1}$. Since, v is a state, v_{k-1} is known. If this acceleration is outside the permissible limits, both v and a are corrected and the corresponding engine speed is calculated. This speed, along with the engine speed and torque at previous time step define the maximum torques $\hat{T}_{e,\max}$ (not $T_{e,\max}$ because turbolag has been considered) and $T_{m,\max}$. To maximize the acceleration, the torque on the engine side of the gearbox is defined as

$$T_{gb,k} = \hat{T}_{e,\max} + T_{m,\max}. \tag{3.9}$$

Now, the torque transmitted at the wheels can be calculated using forward gearbox model. T_w may differ from the initialized torque. So, the procedure is repeated until $T_{w,k}$ and $T_{gb,k}$ are consistent, i.e.

$$T_{gb} - \frac{T_w}{\gamma} < \epsilon. \tag{3.10}$$

The algorithm converges in less than 5 steps with $\epsilon < 0.1$. The outcome of this procedure is that the operation is always at maximum available torque except at times when acceleration is saturated at its maximum limit. The reduced problem can be summarized as follows:

$$x := [v, T_e, n_g], \quad u := [n_g, P_{tc}]$$

Objective:

$$\min \quad -v_N \tag{3.11a}$$

Constraints:

$$v_{k+1} = h(x_k, u_k), \tag{3.11b}$$

$$T_{e,k+1} = l(x_k, u_k), \tag{3.11c}$$

constraints (3.3f)-(3.3m),

$$a_k \leq a_{\max}, \tag{3.11d}$$

$$v_0 = v^0,\ n_{g,0} = n_g^0,\ T_{e,0} = T_e^0, \tag{3.11e}$$

$$\forall\ k \in 0, 1, 2 \ldots N,$$

where h and l are complex nonlinear functions given by the iterative procedure.

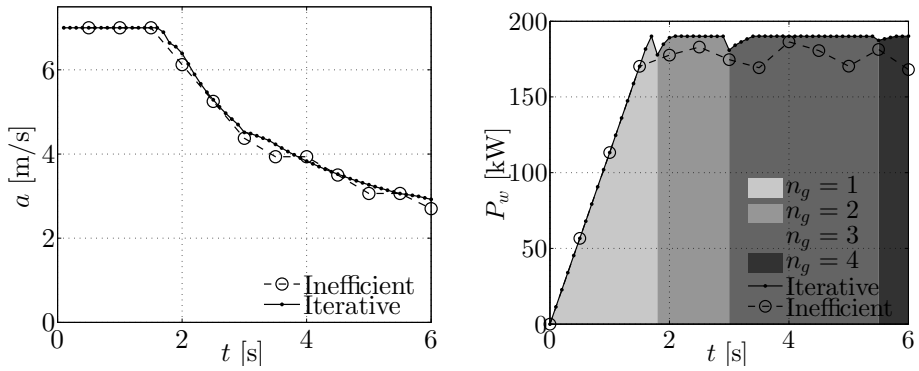

Figure 3.11: Model validation of the iterative procedure (3.11) against the inefficient one (3.5). Acceleration (left) and power delivered at wheels (right).

3.5.3 Model Validation

Problem (3.5) is bound to give an optimal solution and is used to validate this new approach (3.11). The vehicle, initially at rest, is accelerated at full throttle. $a_{\max}$ is $7\,\mathrm{m/s^2}$ and the boost motor has not been used in this comparison. Because of the limitation of the dpm-function in handling the grid size of over 5 million, T_s in (3.5) could not be reduced below 0.5 s, while in (3.11), it is 0.1 s.

Fig. 3.11 shows the comparison for acceleration, power at wheels for the two methods. Initially, the power at wheels is limited by the maximum acceleration and later on by the maximum torque. The active gear number is marked in the background. It is always possible to achieve higher acceleration with the new approach because the power delivered at wheels is more most of the times. The reason is attributed to the refined grid size which was not possible earlier due to numerical complexity.

3.5.4 Results

A comparison is again made between an HEV with a boost motor (Case I) and an HEV without a boost motor (Case II). To accelerate as fast as possible, the tendency of the system is to use maximum torque that is available from both the engine and the traction motor. In Case II, due to turbolag the engine torque cannot be built up fast enough, while in Case I, the boost motor speeds up the turbocharger and as a result more power is instantaneously available from the engine. This effect is illustrated in Fig. 3.12. For instance, at 1 s both the engine speed and engine torque are higher in Case I. The performance analysis is further discussed through standard test criteria. The computation time for 1 simulation in Case I is around 3 min and around 1 min if boost motor is switched off, as in case II.

1. Acceleration at full throttle from 0 to 100 kmph

In this criteria, the time required to accelerate from $0 - 100$ kmph is calculated. The vehicle is initially at rest and is then accelerated at full throttle such that

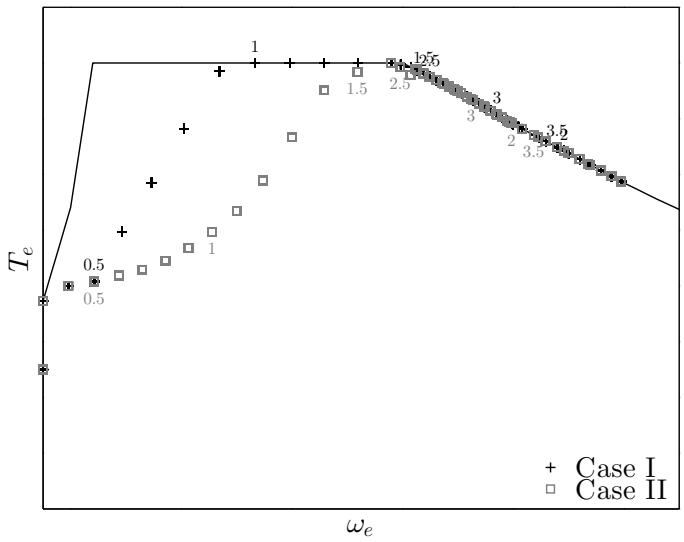

Figure 3.12: Torque-speed trajectory for the two cases while accelerating from 0 kmph to 100 kmph. Time displayed near the markers is in [s]. For first 0.3 s engine is idling at 750 rpm. HEV with the e-boost achieves the maximum torque much faster.

the engine speed is equal to its idling speed at launch. The optimal control inputs along with the vehicle speed are shown in Fig. 3.13. The main difference in the control strategies arise between $0.3 - 0.7$ s. During this time, the boost motor uses 5 kW of electrical power in Case I which leaves aside only 15 kW for the traction motor. Hence, the traction motor torque is less in Case I during this time. The gain in engine power due to reduction in turbolag exceeds the loss in traction motor power which helps to accelerate the vehicle faster. Beyond 0.7 s in Case I and 1.5 s in Case II, the operation is at maximum engine torque or maximum engine power, respectively. Therefore, the turbolag is not observed. Gear shifts in Case I occur earlier because the same vehicle speed is achieved in less time than in Case II. It is worth noting that the boost motor is used after a small delay of 0.3 s at start because until this time the engine speed and the speed of the drivetrain are not synchronized and the engine continues to rotate at the idling speed. The maximum engine torque at the idling speed lies in the naturally aspirated region, and it cannot be increased further by using a boost motor.

2. Acceleration at full throttle from 80 to 120 kmph in 5^{th} gear

In this criteria, the vehicle is assumed to be moving at a constant speed of 80 kmph and is then accelerated at full throttle constantly in the 5^{th} gear. Therefore, only 2 control inputs are required to be optimized. In a higher gear, the acceleration is lower and the vehicle needs more time to accelerate. The simulation results are shown in Fig. 3.14. Again, with the help of the boost motor, the time required to accelerate from $80 - 120$ kmph is less in Case I. The control strategies for the two cases differ mainly between $0 - 0.5$ s when the

boost motor is active. The change in behavior of strategies in both the cases is similar to what is observed in the first test criteria, except now the boost motor is used immediately after start because the engine speed at start is higher than the idling speed.

The results from both of the test criteria are summarized in Tab. 3.6. The time required to accelerate from $0-100$ kmph and $80-120$ kmph is less in Case I by 0.23 s and 0.2 s, respectively. The benefits in acceleration response come at an expense of higher fuel consumption. When the boost motor is used, the engine is forced to operate inefficiently. Note that complete 20 kW of electrical power

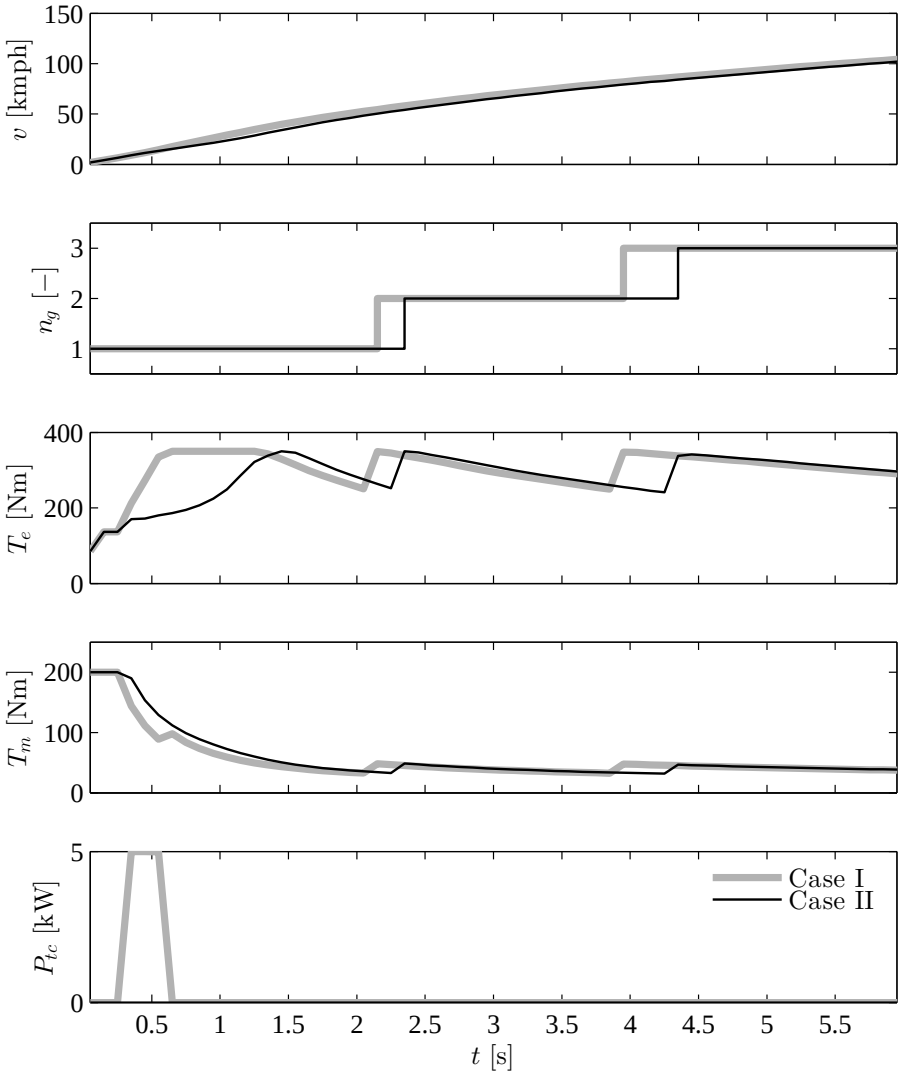

Figure 3.13: Control strategy for minimizing acceleration time in Case I and II while accelerating at full throttle starting from rest. At the end of 6 s, vehicle speed in Case I is 104.19 kmph and in Case II is 101.89 kmph.

Table 3.6: Time required to accelerate, total electrical energy consumed in the mission and the amount of fuel used for Case I (HEV with electrical boost) and Case II (HEV without electrical boost).

		Case I	Case II	Units
$0-100$ kmph	Time lapsed	5.54	5.77	s
	Electrical energy consumed	127.5	134.8	kJ
	Mass of fuel burnt	67.5	66.5	g
$80-120$ kmph	Time lapsed	6.18	6.38	s
	Electrical energy consumed	137.8	142.4	kJ
	Mass of fuel burnt	40.9	40.5	g

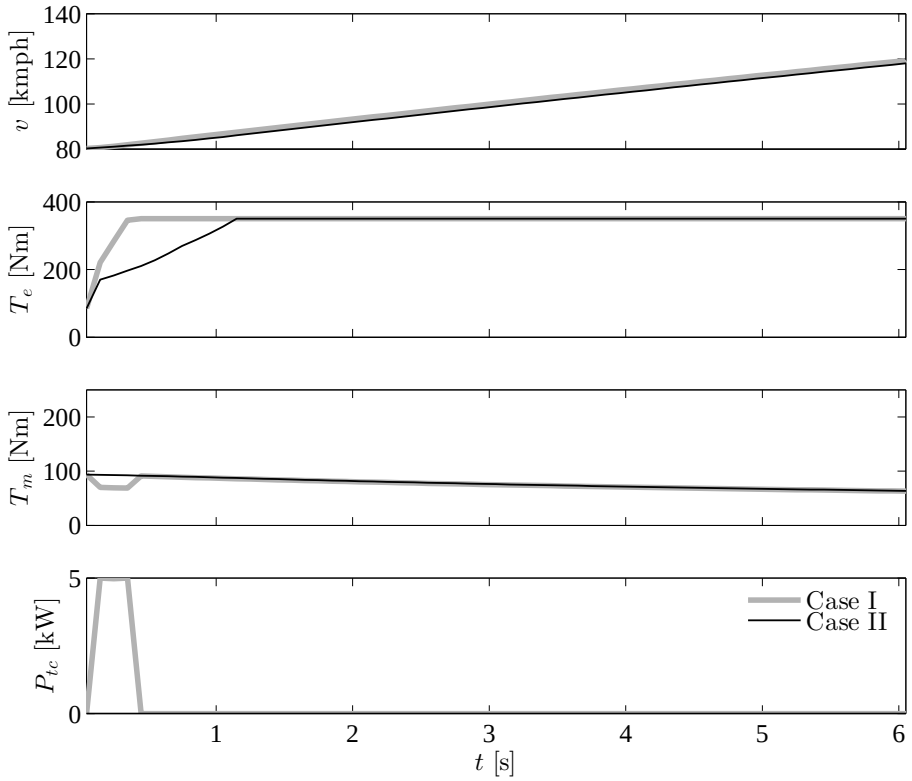

Figure 3.14: Control strategy for minimizing acceleration time in Case I and II while accelerating at full throttle starting from 80 kmph. At the end of 7 s, vehicle speed in Case I is 124.67 kmph and in case II is 123.40 kmph.

is used for the fastest performance in both the cases at each time instant, the only difference being the distribution of this power between the two motors. The electrical energy consumed by the end of mission is less in Case I because the same end speed 100 kmph or 120 kmph is achieved in less time.

The upper limit on acceleration $a_{\max}$ in these tests is limited by g, i.e. $9.81\,\mathrm{m/s^2}$. This can be achieved in a vehicle with four wheel drive or little less than g in only rear wheel drive. This allows us to observe the effects of turbolag very distinctly. The maximum acceleration observed while accelerating from $0-100$ kmph and $80-120$ kmph in Case I is $8.51\,\mathrm{m/s^2}$ and $1.95\,\mathrm{m/s^2}$, respectively, which is infact lower than g. In front wheel drive, typical $a_{\max}$ is around $5\,\mathrm{m/s^2}$. So, third simulation is performed for acceleration from $0-100$ kmph with $a_{\max}=5\,\mathrm{m/s^2}$.

3. Acceleration at full throttle from 0 to 100 kmph with limit on $a_{\max}$

The simulation results are shown in Fig. 3.15. The solutions for both Case I and Case II are identical. Turbolag is observed for $0-1.5$ s and acceleration is saturated at $a_{\max}$ for over 3 s. Even without the boost motor, the power of the traction motor and the engine are sufficient to provide acceleration higher than $5\,\mathrm{m/s^2}$ which eliminates the need of a e-boost mechanism. If size of the traction motor is decreased such that the engine and the motor are incapable of providing this much acceleration, e-boost will again be helpful. This serves as a motivation to study the impact of e-boost in HEVs with different size of traction motors and engines.

3.5.5 Conclusion

The acceleration performance of an HEV with a turbocharged engine can be improved by employing an electric boost mechanism. The boost motor accelerates the turbocharger to overcome turbolag by using a small amount of power from the battery. Since, the total electrical power is constrained to be same as in HEV without boost mechanism, less power is available for the traction motor but the increase in engine torque is more than the decrease in traction motor torque. Thus, at full throttle, an overall increase in driving torque is possible while using the same amount of electrical power which accelerates the vehicle faster. In either test criteria, the optimal control of the boost motor results in a bang-bang solution. It is also evident that the benefits of e-boost can be further magnified with a different choice of engine or motor size.

3.6 Implementation Issues with PMP

Solution method based on Pontryagin's Minimum Principle has been used in the past, often to reduce computation time as well as for online implementation. It requires optimization of a Hamiltonian function H at every time t. For the above model, H can be defined as

$$H(x,u,w)=\dot{m}_f(x,u,w)+\theta_1\,\dot{\xi}(x,u,w)+\theta_2\,\dot{T}_e(x,u,w)+\theta_3\,\dot{\omega}_e(x,u,w). \tag{3.12}$$

The optimal input is then obtained by

$$u^* = \arg\min_u H(x, u, w). \tag{3.13}$$

According to the minimization principle [4], the co-states θ_1, θ_2 and θ_3 can be expressed as

$$\theta_1 = -\frac{\partial H}{\partial \xi},\ \theta_2 = -\frac{\partial H}{\partial T_e},\ \theta_3 = -\frac{\partial H}{\partial \omega_e}. \tag{3.14}$$

In a system with only one state in the form of SoC, only θ_1 must be tuned. Many methods exist for offline and online calculation of θ_1 [9, 20, 30, 47]. Because of

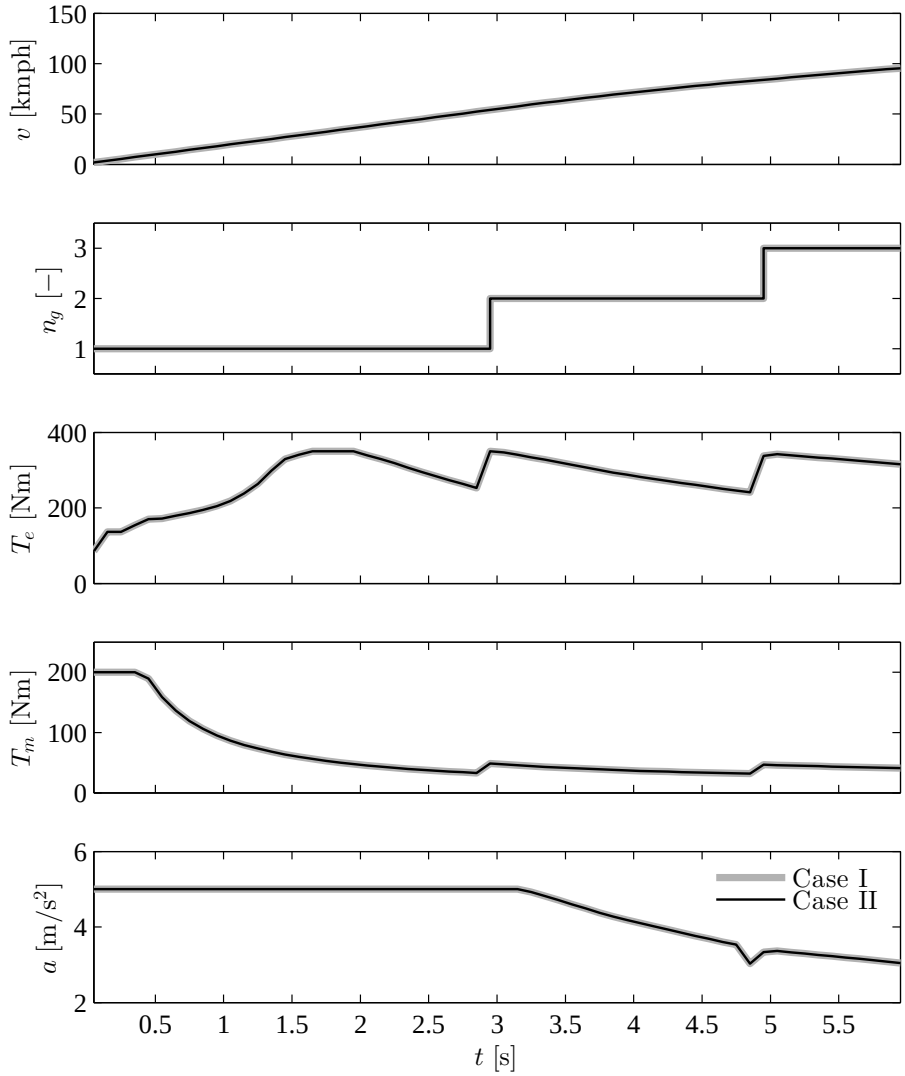

Figure 3.15: Control strategy for minimizing acceleration time in Case I and II while accelerating at full throttle starting from rest, with a cap on maximum acceleration at $5\,\mathrm{m/s^2}$.

the turbolag, the new states T_e and ω_e are inevitable. Therefore, two additional co-states must be tuned in (3.12). In the presence of state constraints, like in this case, one must include corresponding terms in the Hamiltonian which makes it even more complex.

In addition, it can be analytically shown in a single state system that θ_1 can be kept constant because the dynamics of the only state ξ can be assumed to be independent of ξ. Even though this assumption still holds now for θ_1, nothing can be said about θ_2 and θ_3 because $\dot{\xi}$, $\dot{T}_e$ and $\dot{\omega}_e$ are all functions of T_e and ω_e, and their analytical derivation is not straight forward. For instance, for calculation of θ_2, one needs numerical derivative of fuel consumption map and permissible torque map which must be calculated using finite difference method.

Dynamic Programming can also be used to calculate the co-states for offline implementation of PMP using the relations

$$\theta_{1,k} = \left.\frac{\partial J_k(x_k)}{\partial \xi_k}\right|_{x_k^*}, \ \theta_{2,k} = \left.\frac{\partial J_k(x_k)}{\partial T_{e,k}}\right|_{x_k^*}, \ \theta_{3,k} = \left.\frac{\partial J_k(x_k)}{\partial \omega_{e,k}}\right|_{x_k^*}. \tag{3.15}$$

Due to time limitation, the suitability of this method has not been verified.

Chapter 4

Powertrain Sizing

The results presented so far are specific to a set of model parameters. It was observed that the reduction in fuel consumption is not substantial and it is possible only in extreme circumstances but the acceleration performance could be significantly improved. The extent of benefits may also depend on relative size of the powertrain components and the performance may be further improved in an HEV with a different choice of engine or motor. Therefore, the goal of this chapter is to investigate the influence of powertrain component sizes, in particular of the engine displacement volume, the size of the turbocharger and the traction motor power, on the control strategy. This will help to ascertain whether a boost motor should/shouldn't be used with a given combination of engine and traction motor.

4.1 Component Scaling

The reference model discussed till this point has a 2 l engine with a medium size turbocharger (TC) and traction motor with maximum power 20 kW. Now, the performance will be analyzed by selecting different combination of engine and motor from Tab. 4.1. In total, this gives a set of 9 vehicle models. A boost motor capable of providing upto 5 kW, a battery with energy storage capacity 1.2 kWh, and other powertrain components are same in all the models.

Table 4.1: Different sizes of engine and traction motor used for performance comparison. The reference model described so far is shown in bold.

		Traction Motor		
		10 kW	20 kW	40 kW
ICE & TC	small ICE, big TC	M^{11}	M^{21}	M^{31}
	2 l reference model	M^{12}	$\mathbf{M^{22}}$	M^{32}
	big ICE, small TC	M^{13}	M^{23}	M^{33}

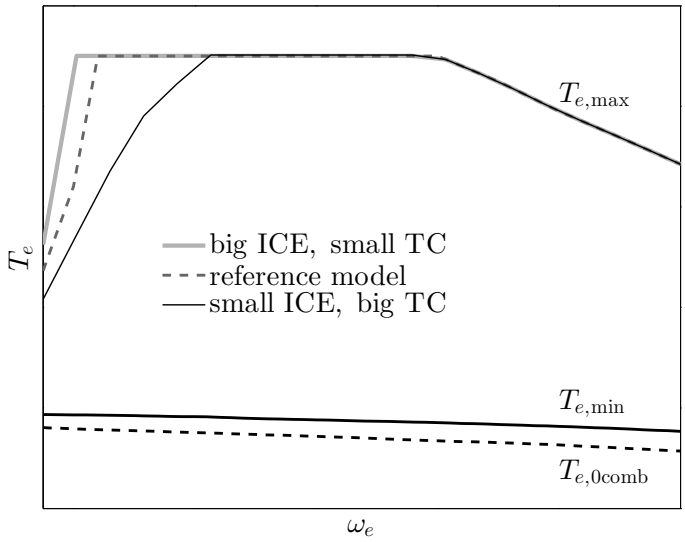

Figure 4.1: Scaled engine maps with different displacement volume and size of the turbocharger. $T_{e,\min}$ and $T_{e,0\text{comb}}$ is same in all the cases.

4.1.1 Internal Combustion Engine

All the 3 engines can provide same maximum power 155 kW and same maximum torque 350 Nm. The difference lies in the displacement volume of engine and the size of turbocharger. The displacement volume of the small engine is less than 2 l. It uses a bigger turbocharger (referred to as BTC in models M^{i1}) and takes the longest time to reach the reference torque, where $i \in \{1, 2, 3\}$. The big engine has a larger displacement volume and uses a smaller turbocharger (referred to as STC in models M^{i3}) to achieve the same maximum torque.

The engines were scaled under expert guidance and using the same measurements from the reference engine described earlier in Tab. 2.1. The corresponding engine maps have been shown in Fig. 4.1. In models M^{i1}, approximately 120 Nm is achieved without any turbolag, while in M^{i3} 200 Nm can be achieved. The torque response of the 3 engines for a particular case is shown in Fig. 4.2. The bigger the size of the turbocharger the larger is its inertia and more is the lag in achieving the reference torque. The maps for the permissible torque for the scaled engines have been attached in Appendix A.

4.1.2 Motor

Three different motors of sizes 10 kW, 20 kW and 40 kW have been used for the comparison. The torque-speed characteristics of the 3 motors are shown in Fig. 4.3. Two motors with maximum power 20 kW and 40 kW were available. The map of 10 kW motor has been obtained by scaling down the map of 20 kW motor by a factor of 0.5.

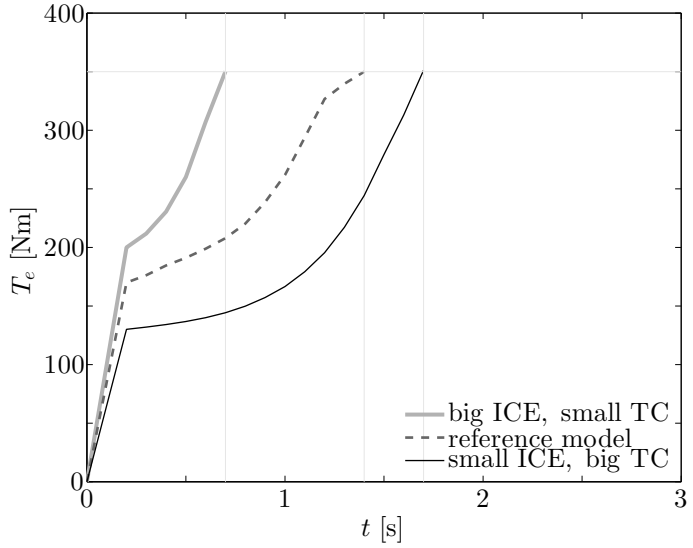

Figure 4.2: Torque response of different engines at full throttle in first gear starting from 8 kmph, (n_g^1, v^8). Time to reach the maximum torque increases with the size of the turbocharger.

4.2 Sizing Study

In the following text, the performance of all the models is evaluated through 3 tests. 2 of these are same as before, i.e. (i) accelerating from $0 - 100$ kmph with optimal gear strategy, and (ii) from $80 - 120$ kmph in the 5^{th} gear. In (i) the starting engine speed is equal to the idling speed which is referred to as idle start. So, the clutch plates slip against each other until the speed of the

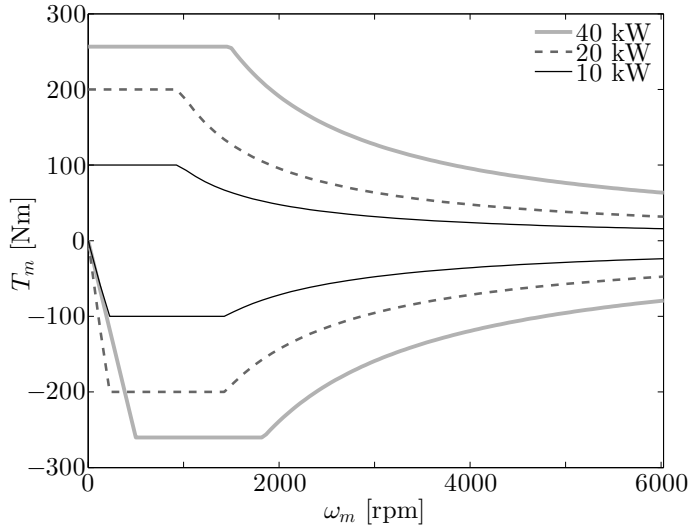

Figure 4.3: Torque-speed characteristics of the considered traction motors.

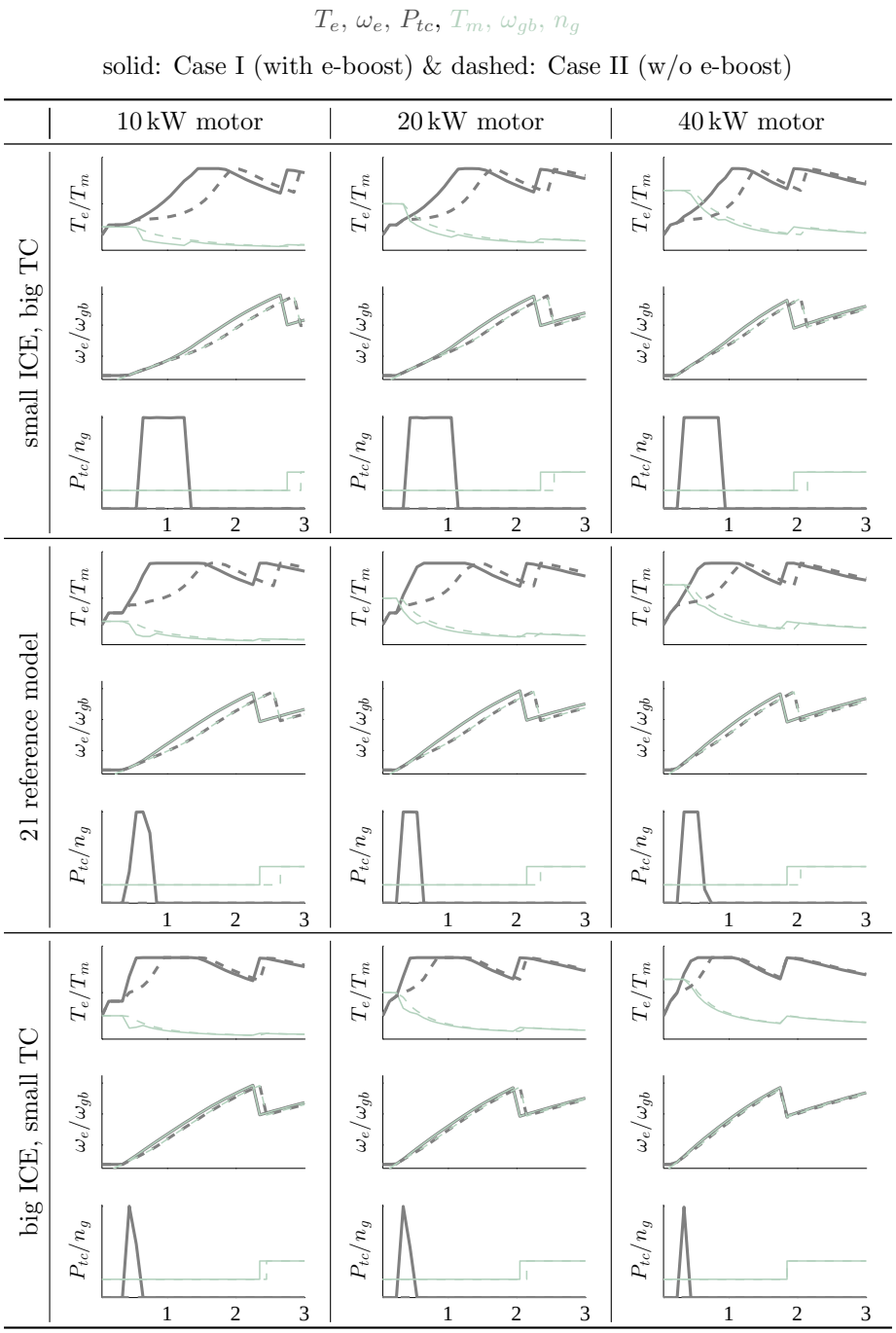

Figure 4.4: Simulations for performance comparison for different combination of engine and traction motor sizes while accelerating from $0 - 100$ kmph with idle start. On the x-axis is time in [s]. For clarity, only first 3 s are shown which includes only one gear shift, from 1 to 2.

drivetrain shaft attains the idling speed. A special case of (i) is also discussed when the launch speed of the engine is higher than the idling speed, taken as 1500 rpm here. This is called as non-idle start. At higher launch speed, the engine experiences less turbolag and is capable of providing higher initial torque.

Both qualitative and quantitative analysis of results have been presented for 2 scenarios described in Tab. 3.1 for various models discussed in Tab. 4.1.

1. Acceleration at full throttle from 0 to 100 kmph with idle start

The influence of different sizes of the engine and the traction motor is shown in Fig. 4.4. With any size of the engine or the motor, the acceleration performance in Case I is better than Case II, however the amount of benefits vary with the size. This can also be observed from the gear up-shift pattern. Except for the case with the big engine (STC) and the big motor (40 kW), the gear shift from 1 to 2 occurs earlier in Case I because the same engine speed is reached earlier. The optimal control of electrical boost P_{tc} in most of the models results in a bang-bang solution, i.e. switching digitally between 0 kW and 5 kW. It lies between $0-5$ kW only if the engine torque cannot be increased further by using more boost power, for instance at 0.6 s in the model with the reference engine and 40 kW motor.

In Case I, for any combination of engine and motor size, it is observed that the boost motor is used after a small delay at start, $0.2 - 0.5$ s depending upon the model. During this time, the clutch is slipping and the engine rotates at its idling speed. The engine delivers torque corresponding to maximum torque at this speed which lies in the naturally aspirated region of the engine map. So, the boost motor is not functional until the engine speed and the drivetrain speed are synchronized.

For a fixed engine size, this delay decreases with an increase in traction motor size. A bigger motor can deliver higher torque, so the acceleration is more at start up and the speed of the drivetrain and the engine match earlier. Also, because of higher motor torque, the vehicle has higher speed and observes less turbolag. So, the maximum engine torque is reached earlier which has influence on duration for which the boost motor is used in the optimal strategy. Specifically, consider the case with the small engine and big turbocharger. Duration for which the boost motor is used is less for 40 kW motor than 20 kW motor.

For a fixed motor size, the benefits of the boost mechanism are the most visible with the smallest engine. Because of higher turbolag, the boost motor is used for a longer duration. This time decreases with an increase in size of the engine. Correspondingly, the time required to reach 100 kmph is not much affected by the boost mechanism in the big engine with less turbolag.

The time required T to achieve 100 kmph, for all the models, is shown in Fig. 4.5. The maximum absolute reduction in T is seen with the small traction motor (10 kW). % reduction in T is comparable for the small engine with big turbocharger (BTC) and the reference model (RTC) for all motor sizes and it is much less for the big engine with small turbocharger (STC). For a given engine,

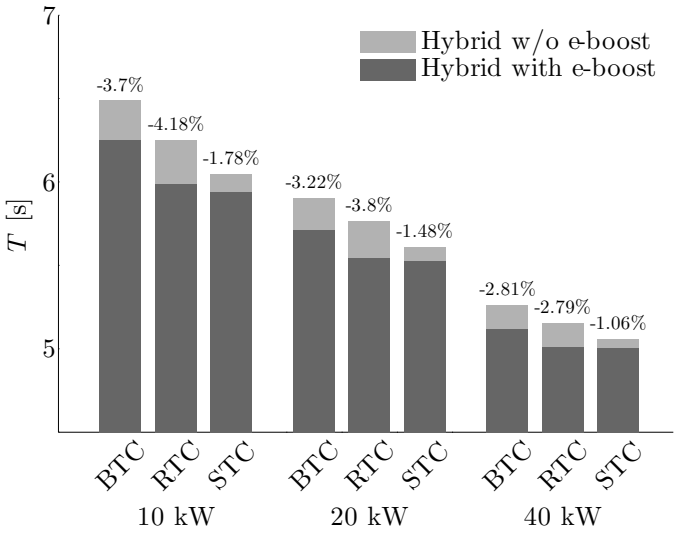

Figure 4.5: Time required to achieve 100 kmph in Case I and Case II for different models with idle start. Number over the bars shows percent reduction in time due to e-boost.

% reduction in T decreases with an increase in size of the motor.

2. Acceleration at full throttle from 0 to 100 kmph with non-idle start

The simulations for this test are shown in Fig. 4.7. Again, the acceleration

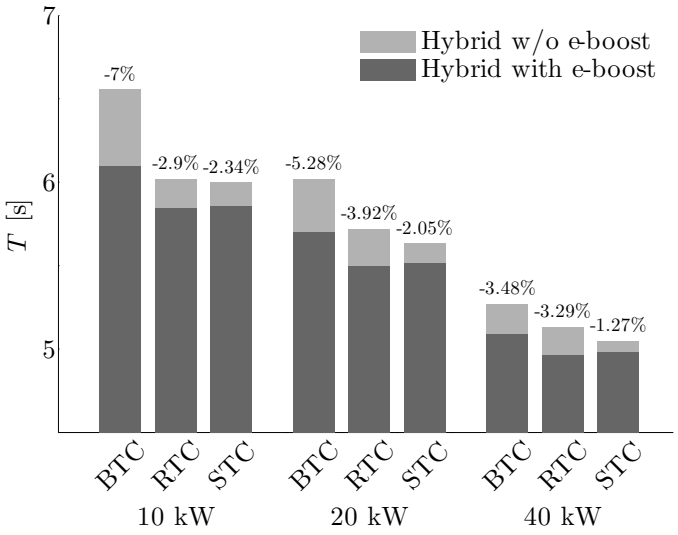

Figure 4.6: Time required to achieve 100 kmph in Case I and Case II for different models with non-idle start. Number over the bars shows percent reduction in time due to e-boost.

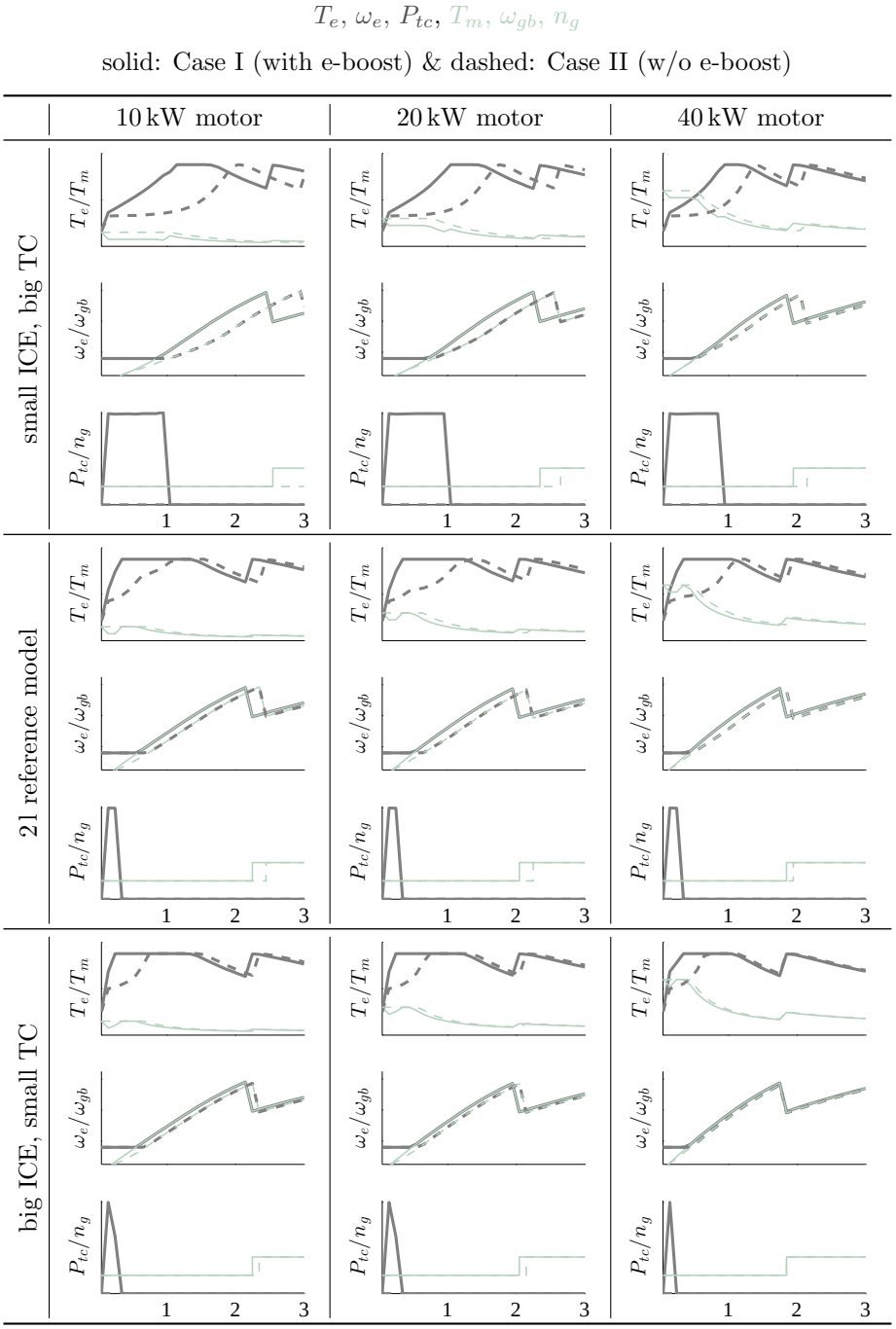

Figure 4.7: Simulations for performance comparison for different combination of engine and traction motor sizes while accelerating from $0 - 100$ kmph with non-idle start at 1500 rpm. On the x-axis is time in [s]. For clarity, only first 3 s are shown which includes only one gear shift, from 1 to 2.

performance is improved in each model. Qualitatively, the results are same as that in Fig. 4.4, except that the engine speed now at start is 1500 rpm which facilitates the boost motor to be used immediately after start. It is again observed that the boost motor is used for a longer duration with the smaller engine for any motor size. This effect is less pronounced in the direction of increasing motor size for a fixed type of engine.

The time required T to achieve 100 kmph is shown in Fig. 4.6. T with non-idle start can be more or less than T with idle start depending upon the size of motor, see Appendix B. The motor size plays an important role now because of the reasons mentioned therein. Nevertheless, it shows that the boost motor is used immediately after start in the case of non-idle start. In most of the models, % reduction in T is more with non-idle start because the initial delay in action of the boost motor, as seen in the case of idle start, doesn't exist anymore. Again, high reduction in T can be achieved with small/medium sized engine and $10-20$ kW motor. This number is less in the case of a bigger engine. Because of scaling, comparison of absolute numbers between different engines with the same motor is not advisable.

3. Acceleration at full throttle from 80 to 120 kmph in 5^{th} gear

Fig. 4.9 and 4.8 show the same trends in the results as discussed before. The only difference lies in the time taken from $80-120$ kmph. Acceleration is low in high gears, so much higher time is required for the same gain in speed.

Thus, in principle, it can be concluded that the boost mechanism in an HEV improves performance, irrespective of the model size and performance criteria. In comparison to the reference model, magnitude of benefits is less with a relatively smaller turbocharger and more with a smaller traction motor.

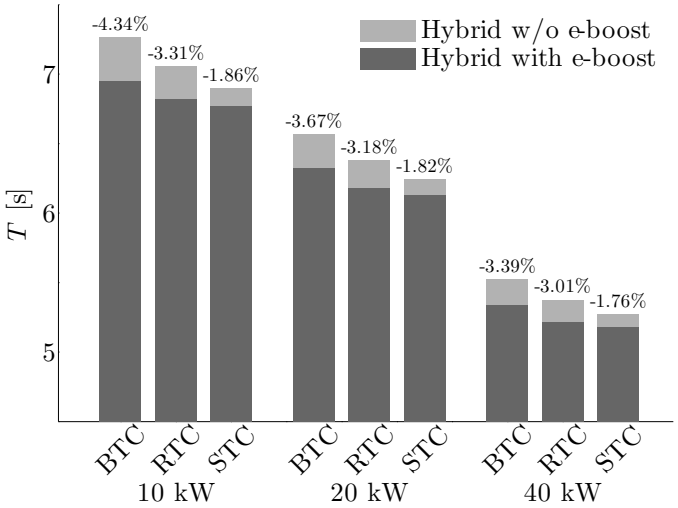

Figure 4.8: Time required to achieve 120 kmph in Case I and Case II for different models. Number over the bars shows percent reduction in time due to e-boost.

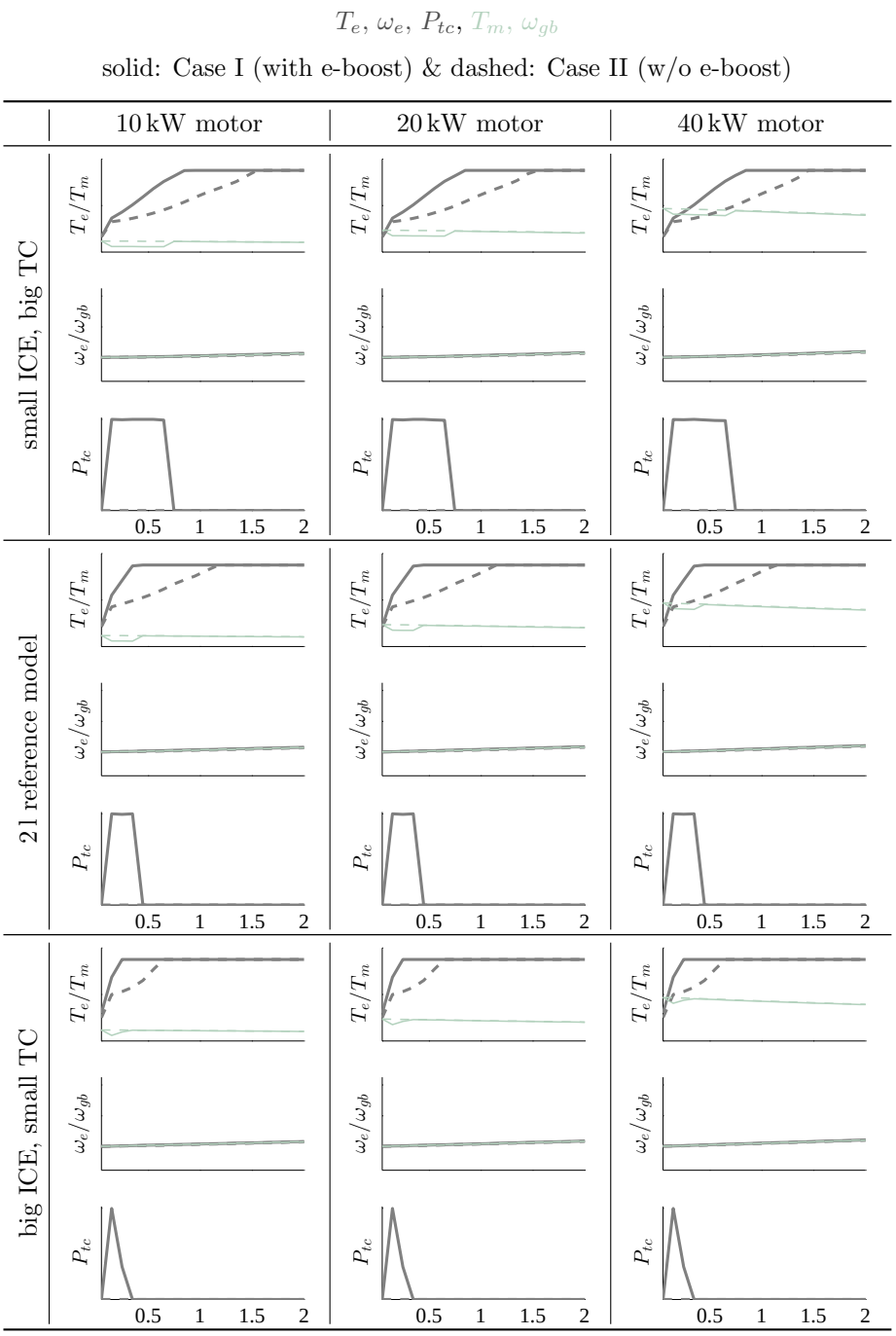

Figure 4.9: Simulations for performance comparison for different combination of engine and traction motor sizes while accelerating from $80 - 120$ kmph in 5^{th} gear. On the x-axis is time in [s]. For clarity, only first 2 s are shown.

4.3 Robustness Analysis

To this end, a simple model of the system has been developed. It was further scaled to study the impact of size of traction motor and engine. In the whole process, many assumptions were made both in modeling and scaling. As a final step, this scaled system is tested with very low efficiency of the boost mechanism to examine the robustness of the system. Now, η_{tc} has been chosen to be 0.4, instead of 0.75 which was used earlier. Specifically, comparisons have been done for Case I with high η_{tc} and Case I with low η_{tc} in 2 tests: $0 - 100$ kmph with idle start and $80 - 120$ kmph in 5^{th} gear. These simulations are shown in Fig. 4.11 and 4.12.

Low efficiency of the boost mechanism means that with a power demand of 5 kW, the boost motor can provide only 2 kW for reducing the turbolag. So, this system takes longer time to reach the maximum engine torque because less power is available at every time step. Irrespective of the model size, this effect is visible in Fig. 4.11 and 4.12. The result is that the boost motor is used for a longer duration. For Fig. 4.11, the comparison of the final time is presented in Fig. 4.10. Evidence that the optimal strategy prefers to reduce turbolag with e-boost even with such low efficiency of the boost mechanism confirms the robustness of the model despite many assumptions.

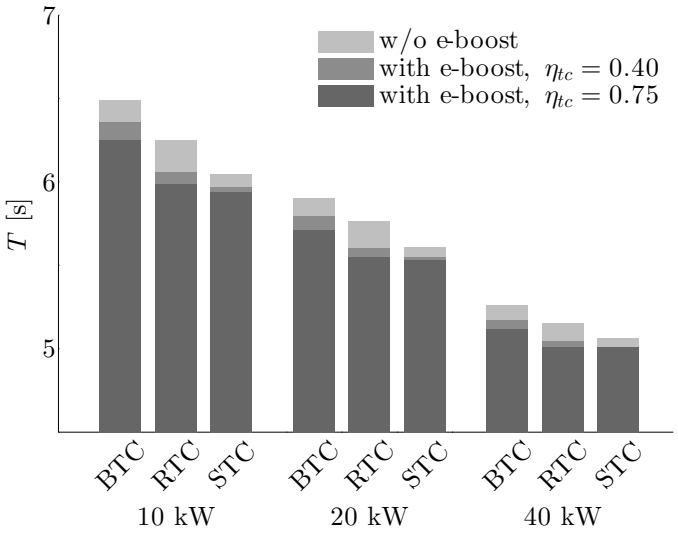

Figure 4.10: Time required to achieve 100 kmph in Case I with high η_{tc}, Case I with low η_{tc} and Case II (w/o e-boost) for different models with idle start.

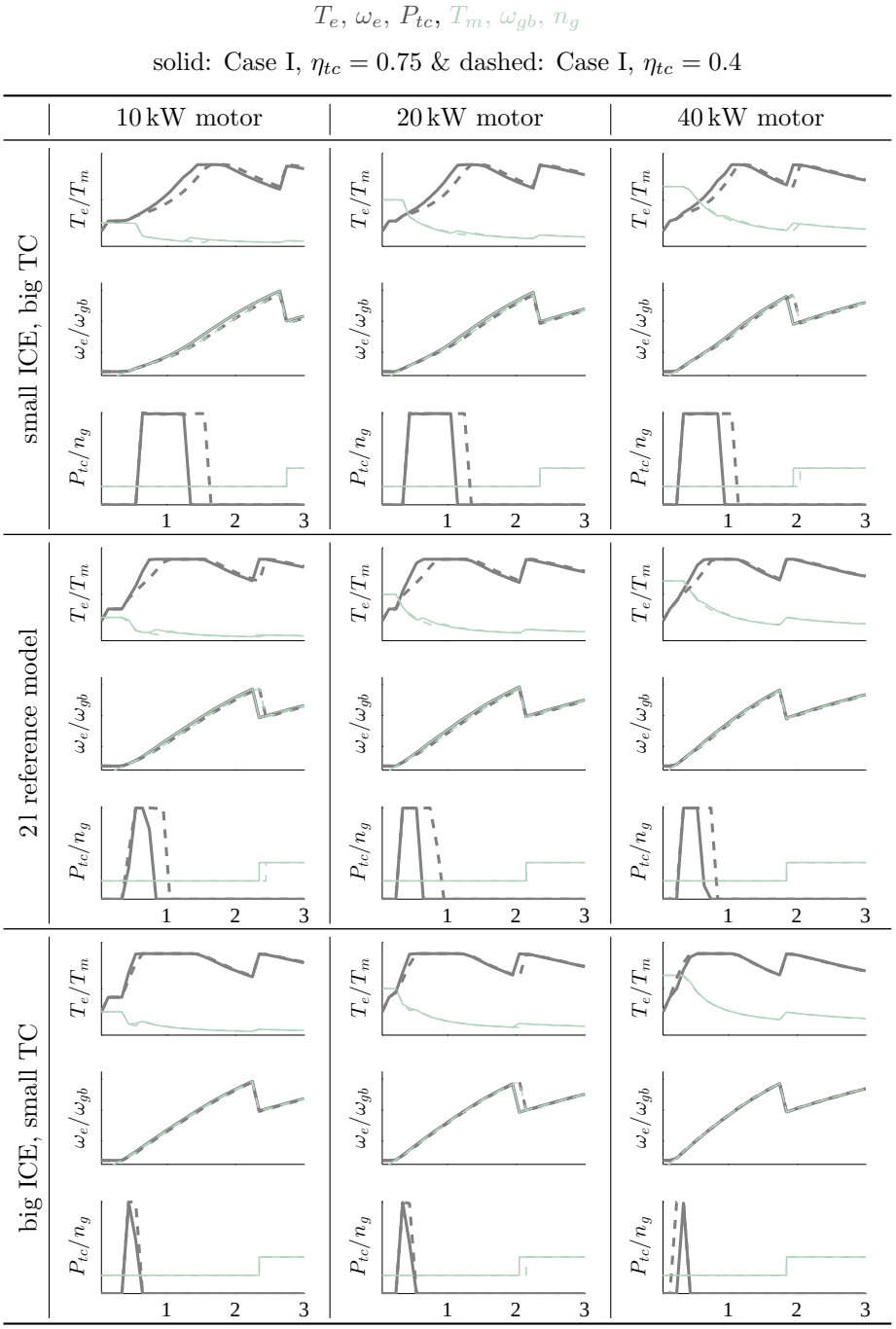

Figure 4.11: Simulations for performance comparison for different combination of engine and traction motor sizes while accelerating from $0 - 100$ kmph with idle start. On the x-axis is time in [s]. For clarity, only first 3 s are shown which includes only one gear shift, from 1 to 2.

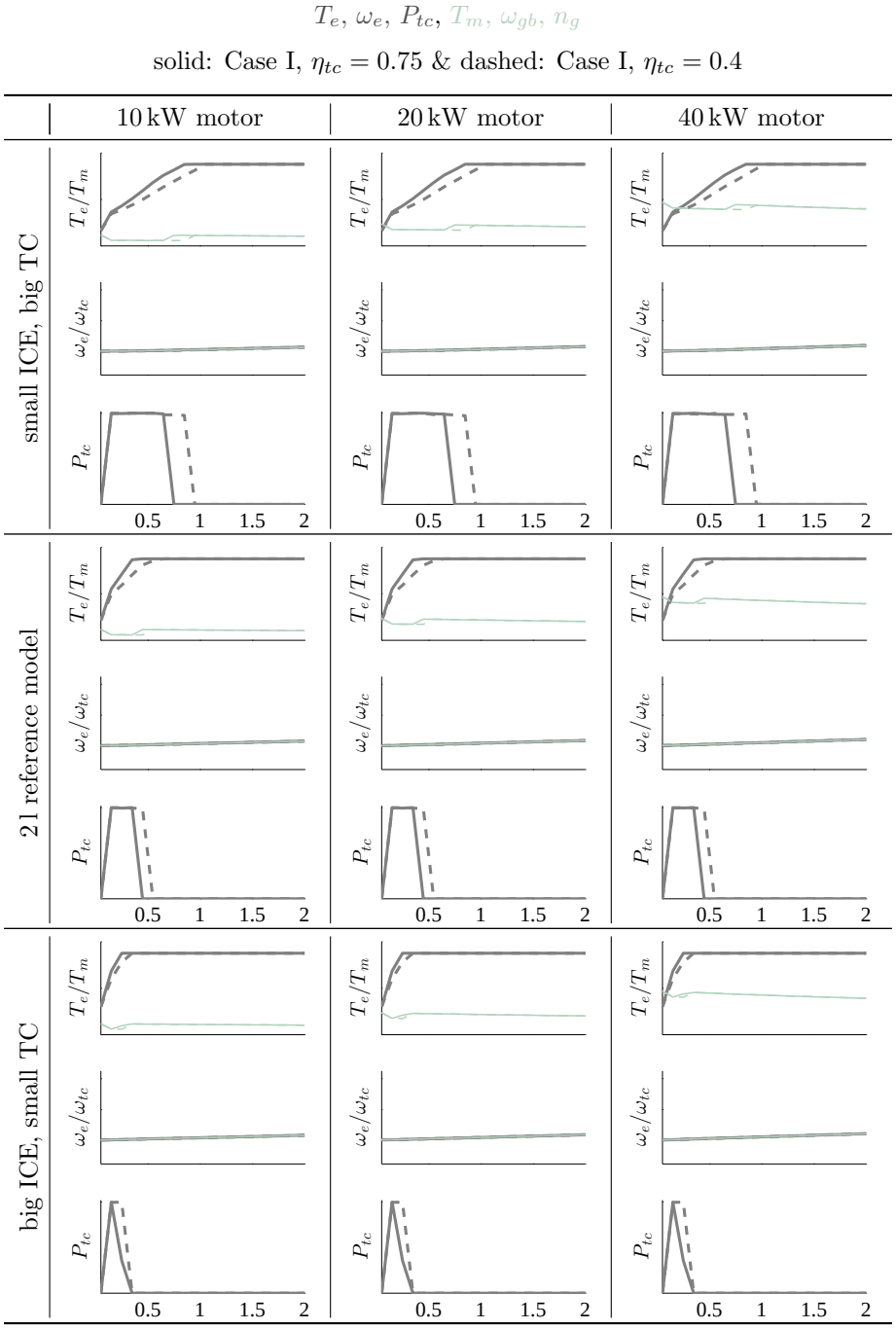

Figure 4.12: Simulations for performance comparison for different combination of engine and traction motor sizes while accelerating from $80 - 120$ kmph in 5^{th} gear. On the x-axis is time in [s]. For clarity, only first 2 s are shown.

Chapter 5

Conclusion

Energy management in an HEV with an electrically assisted turbocharger in P1 topology has been studied. A framework to model and solve the optimal control problem has been established. Dynamic Programming is used to solve this problem for optimizing performance with respect to fuel consumption and acceleration response, the control variables being the torque split between the engine and the electric motor, the amount of electrical turbocharging and the gear number.

The boost motor does not offer any advantages in the real world driving cycles, mainly because the torque demand in these cycles is too low and only a few operating points lie in the turbocharged region of the engine map. Even under high torque requirements, boost motor offers only theoretical benefits over a conventional HEV in reducing the fuel consumption. Thus, it is not recommended to use an electrically assisted turbocharger for the sake of only fuel economy. One potential advantage of using a boost motor is the capability to recharge the battery when load requirements are too high and recuperation is not possible otherwise.

The acceleration response of an HEV can be improved substantially by using an electrically assisted turbocharger. This has been verified through simulations in two standard test criteria, namely accelerating from 0 to 100 kmph with an optimal gear strategy and from 80 to 120 kmph in a fixed gear. However, better acceleration response comes at an expense of higher fuel consumption. The usefulness of a boost motor also depends on relative size of powertrain components. A theoretical investigation suggests that the magnitude of benefits increase with reduction in size of the traction motor, and decrease with an engine using a bigger turbocharger and providing the same maximum torque and power as the reference engine. Lastly, the robustness of the proposed model has also been verified by varying the efficiency of the boost mechanism.

In this project, the electric machine coupled to the turbocharger works only in motor mode. Using it in generator mode as well could potentially decrease the fuel consumption, but it needs more research. Also, the scaling of engine is very theoretical and could not be validated. Nevertheless, the results are well found and it opens avenues for future work.

Appendix A

Permissible Torque Maps for the Scaled Engines

A.1 Small ICE, Big TC

The engine has displacement volume less than 2l. With the help of a more powerful turbocharger, same maximum torque and maximum power (as of the reference engine) can be achieved. Because of higher inertia of the turbocharger, more turbolag is expected. Consequently, the permissible torque values are low.

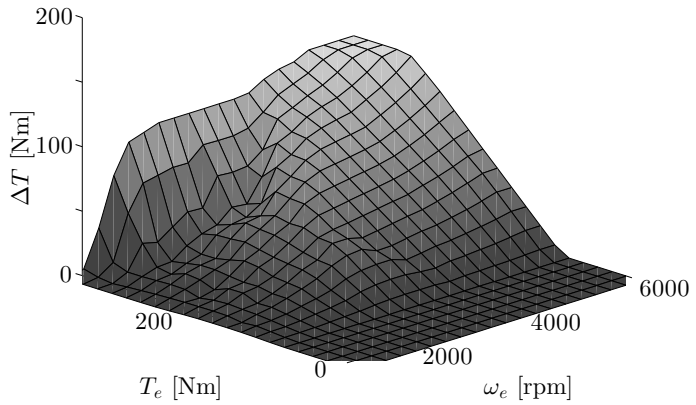

Figure A.1: Map of permissible torque for the small engine with big turbocharger.

A.2 Big ICE, Small TC

The engine has displacement volume more than 2l. This engine needs a smaller turbocharger to achieve the same maximum torque and maximum power (as of

the reference engine). In this case, less turbolag is expected because the inertia of the turbocharger is also smaller. Hence, the values of the permissible torque are higher.

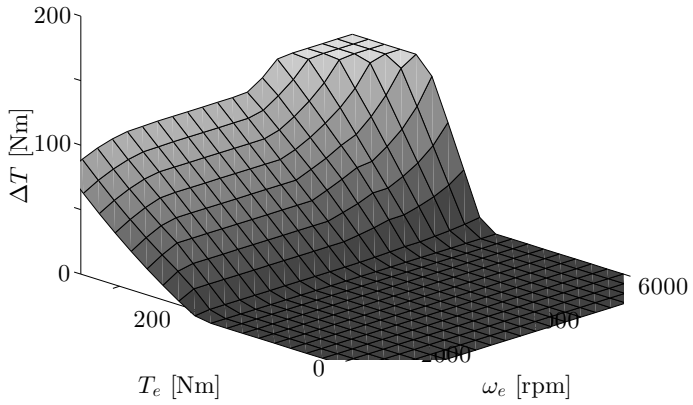

Figure A.2: Map of permissible torque for the big engine with small turbocharger.

Appendix B

Analysis of non-idle start behaviour

In a conventional vehicle where ICE is the only source of power, the time required to accelerate reduces significantly with the non-idle start, or more commonly known as the race start when the launch speed is as high as 4000 rpm. HEVs do not show this typical acceleration behavior with the non-idle start. Especially in P1 configuration where the ICE and the traction motor rotate at a same speed, the non-idle start reduces the initial motor torque and the motor continues to rotate at low torque until the speed of the engine and the drivetrain are synchronized. Although, the turbolag is less with the non-idle start, but the reduction in motor torque causes the system to underperform in the initial phase of acceleration. Fig. B.1 (L) shows the acceleration of the reference model for the two cases at the same initial torque. It can be seen that the acceleration is higher with the idle start until both reach the maximum engine torque. Due to this fact, the time required to accelerate with the non-idle start and the idle start at low engine torque can be similar. Fig. B.1 (R) further explains this observation. The sum of $T_{e,\max}$ and $T_{m,\max}$ is plotted against the engine speed. The peak of this curve lies close to the idle speed. Thus, starting very far from the peak can degrade the acceleration peformance in HEVs.

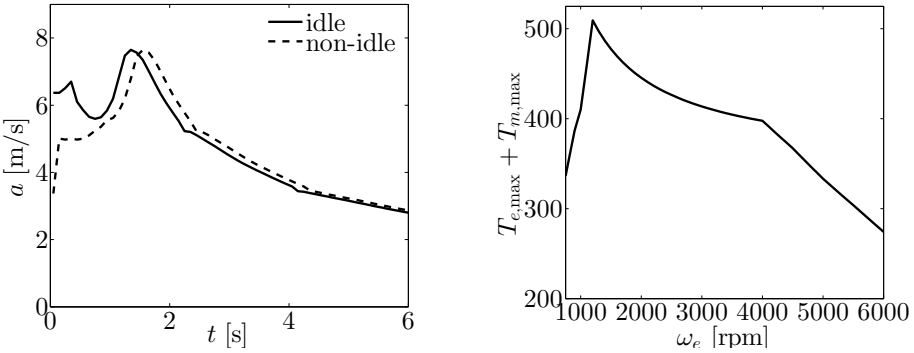

Figure B.1: Acceleration comparison between idle and non-idle start (L) and sum of maximum engine and motor torque (R).

Bibliography

[1] Ivan Arsie, Andrea Cricchio, Cesare Pianese, Matteo De Cesare, and Walter Nesci. A comprehensive powertrain model to evaluate the benefits of electric turbo compound (etc) in reducing co2 emissions from small diesel passenger cars. Technical report, SAE Technical Paper, 2014.

[2] Michael Back. *Prädiktive Antriebsregelung zum energieoptimalen Betrieb von Hybridfahrzeugen*. Univ.-Verlag Karlsruhe, 2005.

[3] John C Bass, Aleksandr S Kushch, and Norbert B Elsner. Thermoelectric generator (teg) for heavy diesel trucks. In *International Conference on Thermoelectrics: Proceedings ICT2001*, 2001.

[4] Dimitri P Bertsekas, Dimitri P Bertsekas, Dimitri P Bertsekas, and Dimitri P Bertsekas. *Dynamic programming and optimal control*, volume 1. Athena Scientific Belmont, MA, 1995.

[5] Daniel Boland, Hans-Juergen Berner, and Michael Bargende. Optimization of a cng driven si engine within a parallel hybrid power train by using egr and an oversized turbocharger with active-wg control. *Future*, 2013:04–08, 2010.

[6] Hoseinali Borhan, Ardalan Vahidi, Anthony M Phillips, Ming L Kuang, Ilya V Kolmanovsky, and Stefano Di Cairano. Mpc-based energy management of a power-split hybrid electric vehicle. *Control Systems Technology, IEEE Transactions on*, 20(3):593–603, 2012.

[7] I Briggs, G McCullough, S Spence, R Douglas, et al. Waste heat recovery on a diesel-electric hybrid bus using a turbogenerator. *Training*, 2005:07–01, 2012.

[8] Jim Bumby, Sue Crossland, and Jeff Carter. Electrically assisted turbochargers: their potential for energy recovery. In *Hybrid Vehicle Conference, IET The Institution of Engineering and Technology, 2006*, pages 43–52. IET, 2006.

[9] Alexandre Chasse, Philippe Pognant-Gros, and Antonio Sciarretta. Online implementation of an optimal supervisory control for a parallel hybrid powertrain. Technical report, SAE Technical Paper, 2009.

[10] Steven Chu and Arun Majumdar. Opportunities and challenges for a sustainable energy future. *nature*, 488(7411):294–303, 2012.

[11] Thomas E Darlington and Andrew A Frank. Exhaust gas driven generator with altitude compensation for battery dominant hybrid electric vehicles. In *ASME 2004 Internal Combustion Engine Division Fall Technical Conference*, pages 1–10. American Society of Mechanical Engineers, 2004.

[12] Sebastien Delprat, Jimmy Lauber, Thierry-Marie Guerra, and Janette Rimaux. Control of a parallel hybrid powertrain: optimal control. *Vehicular Technology, IEEE Transactions on*, 53(3):872–881, 2004.

[13] Stefano Di Cairano, Wei Liang, Ilya V Kolmanovsky, Ming L Kuang, and Anthony M Phillips. Power smoothing energy management and its application to a series hybrid powertrain. *Control Systems Technology, IEEE Transactions on*, 21(6):2091–2103, 2013.

[14] Rutger Dijkstra, Michael Boot, Ruud Eichhorn, David Smeulders, Johan Lennblad, and Alexander Serrarens. Experimental analysis of engine exhaust waste energy recovery using power turbine technology for light duty application. *SAE International Journal of Engines*, 5(4):1729–1739, 2012.

[15] Prasad Sajjan Divekar, Beshah Ayalew, and Robert Prucka. Coordinated electric supercharging and turbo-generation for a diesel engine. Technical report, SAE Technical Paper, 2010.

[16] V Dolz, R Novella, A García, and J Sánchez. Hd diesel engine equipped with a bottoming rankine cycle as a waste heat recovery system. part 1: study and analysis of the waste heat energy. *Applied Thermal Engineering*, 36:269–278, 2012.

[17] Philipp Elbert, Soren Ebbesen, and Lino Guzzella. Implementation of dynamic programming for-dimensional optimal control problems with final state constraints. *Control Systems Technology, IEEE Transactions on*, 21(3):924–931, 2013.

[18] Lars Eriksson, Lars Nielsen, Jan Brugård, Johan Bergström, Fredrik Pettersson, and Per Andersson. Modeling of a turbocharged si engine. *Annual Reviews in Control*, 26(1):129–137, 2002.

[19] Frank G Gerke. Diesel engine waste heat recovery utilizing electric turbocompound technology. Technical report, 2001.

[20] BO Gu and Giorgio Rizzoni. An adaptive algorithm for hybrid electric vehicle energy management based on driving pattern recognition. In *ASME 2006 International Mechanical Engineering Congress and Exposition*, pages 249–258. American Society of Mechanical Engineers, 2006.

[21] Lino Guzzella and Christopher Onder. *Introduction to Modeling and Control of Internal Combustion Engine Systems*. Springer, 2010.

[22] Lino Guzzella and Antonio Sciarretta. *Vehicle propulsion systems*, volume 2. Springer, 2013.

[23] Hongwen He, Xiaowei Zhang, Rui Xiong, Yongli Xu, and Hongqiang Guo. Online model-based estimation of state-of-charge and open-circuit voltage of lithium-ion batteries in electric vehicles. *Energy*, 39(1):310–318, 2012.

[24] Ulrich Hopmann and Marcelo C Algrain. Diesel engine electric turbo compound technology. *Diesel Engine*, 2013:04–08, 2003.

[25] DT Hountalas, CO Katsanos, and VT Lamaris. Recovering energy from the diesel engine exhaust using mechanical and electrical turbocompounding. Technical report, SAE Technical Paper, 2007.

[26] Y Ismail, D Durrieu, P Menegazzi, P Chesse, et al. Potential of exhaust heat recovery by turbocompounding. *Diesel Engine*, 2012:12–04, 2012.

[27] JP Jensen, AF Kristensen, Spencer C Sorenson, N Houbak, and E Hendricks. Mean value modeling of a small turbocharged diesel engine. *Training*, 2014:04–11, 1991.

[28] Lars Johannesson, Mattias Asbogard, and Bo Egardt. Assessing the potential of predictive control for hybrid vehicle powertrains using stochastic dynamic programming. *Intelligent Transportation Systems, IEEE Transactions on*, 8(1):71–83, 2007.

[29] Tomai Katrašnik, Samuel Rodman, Ferdinand Trenc, Aleš Hribernik, and Vladimir Medica. Improvement of the dynamic characteristic of an automotive engine by a turbocharger assisted by an electric motor. *Journal of engineering for gas turbines and power*, 125(2):590–595, 2003.

[30] John TBA Kessels, Michiel WT Koot, Paul PJ van den Bosch, and Daniel B Kok. Online energy management for hybrid electric vehicles. *IEEE Transactions on vehicular technology*, 57(6):3428–3440, 2008.

[31] Namwook Kim, Sukwon Cha, and Huei Peng. Optimal control of hybrid electric vehicles based on pontryagin's minimum principle. *Control Systems Technology, IEEE Transactions on*, 19(5):1279–1287, 2011.

[32] Ilya Kolmanovsky, P Morall, Michiel Van Nieuwstadt, and Anna Stefanopoulou. Issues in modelling and control of intake flow in variable geometry turbocharged engines. *Chapman and Hall CRC research notes in mathematics*, pages 436–445, 1999.

[33] Ilya Kolmanovsky and Anna G Stefanopoulou. Evaluation of turbocharger power assist system using optimal control techniques. *Evaluation*, 1:0519, 2000.

[34] I.V. Kolmanovsky and A.G. Stefanopoulou. Optimal control techniques for assessing feasibility and defining subsystem level requirements: an automotive case study. 9(3):524–534, 2001.

[35] Michiel Koot, John TBA Kessels, Bram de Jager, WPMH Heemels, PPJ Van den Bosch, and Maarten Steinbuch. Energy management strategies for vehicular electric power systems. *Vehicular Technology, IEEE Transactions on*, 54(3):771–782, 2005.

[36] Aleksandr S Kushch, John C Bass, Saeid Ghamaty, and NB Eisner. Thermoelectric development at hi-z technology. In *Thermoelectrics, 2001. Proceedings ICT 2001. XX International Conference on*, pages 422–430. IEEE, 2001.

[37] Chan-Chiao Lin, Huei Peng, Jessy W Grizzle, and Jun-Mo Kang. Power management strategy for a parallel hybrid electric truck. *Control Systems Technology, IEEE Transactions on*, 11(6):839–849, 2003.

[38] Chan-Chiao Lin, Huei Peng, and JW Grizzle. A stochastic control strategy for hybrid electric vehicles. In *American Control Conference, 2004. Proceedings of the 2004*, volume 5, pages 4710–4715. IEEE, 2004.

[39] Federico Millo, Fabio Mallamo, E Pautasso, and G Ganio Mego. The potential of electric exhaust gas turbocharging for hd diesel engines. *SAE Technical Paper*, pages 01–0437, 2006.

[40] Cristian Musardo, Giorgio Rizzoni, Yann Guezennec, and Benedetto Staccia. A-ecms: An adaptive algorithm for hybrid electric vehicle energy management. *European Journal of Control*, 11(4):509–524, 2005.

[41] Tobias Nüesch, Philipp Elbert, Michael Flankl, Christopher Onder, and Lino Guzzella. Convex optimization for the energy management of hybrid electric vehicles considering engine start and gearshift costs. *Energies*, 7(2):834–856, 2014.

[42] Daniel F Opila, Xiaoyong Wang, Ryan McGee, R Brent Gillespie, Jeffrey A Cook, and Jessy W Grizzle. An energy management controller to optimally trade off fuel economy and drivability for hybrid vehicles. *Control Systems Technology, IEEE Transactions on*, 20(6):1490–1505, 2012.

[43] Tobias Ott, Lino Guzzella, and Christopher Harald Onder. How much fuel can a hybrid electric vehicle save? IAMF 2011 full paper, International Advanced Mobility Forum, 2011, Genf, 2011.

[44] P Pallotti, E Torella, J New, M Criddle, and J Brown. Application of an electric boosting system to a small, four-cylinder si engine. Technical report, SAE Technical Paper, 2003.

[45] Pierluigi Pisu and Giorgio Rizzoni. A comparative study of supervisory control strategies for hybrid electric vehicles. *Control Systems Technology, IEEE Transactions on*, 15(3):506–518, 2007.

[46] Antonio Sciarretta and Lino Guzzella. Control of hybrid electric vehicles. *Control systems, IEEE*, 27(2):60–70, 2007.

[47] Antonio Sciarretta, Lino Guzzella, and Michael Back. A real-time optimal control strategy for parallel hybrid vehicles with on-board estimation of the control parameters. In *Proc. IFAC Symp. Adv. Automotive Contr*, pages 19–23, 2004.

[48] Lorenzo Serrao, Antonio Sciarretta, Olivier Grondin, Alexandre Chasse, Yann Creff, Domenico Di Domenico, Philippe Pognant-Gros, Carole Querel, and Laurent Thibault. Open issues in supervisory control of hybrid electric vehicles: a unified approach using optimal control methods. *Oil and Gas Science and Technology - Revue d'IFP Energies nouvelles*, 68(1):23–33, 2013.

[49] Syed M Shahed. An analysis of assisted turbocharging with light hybrid powertrain. *Writing*, 1:1315, 2005.

[50] R Sharma, D Nesic, and C Manzie. Control oriented modeling of turbocharged spark ignition engine. In *SAE World Congress 2009*. SAE International, 2009.

[51] Richard Stobart and Rohitha Weerasinghe. Heat recovery and bottoming cycles for si and ci engines–a perspective. *Training*, 2013:11–19, 2006.

[52] Olle Sundstrom and Lino Guzzella. A generic dynamic programming matlab function. In *Control Applications,(CCA) & Intelligent Control,(ISIC), 2009 IEEE*, pages 1625–1630. IEEE, 2009.

[53] Mercedes AMG Petronas Formula One Team. Pu 106a hybrid. http://www.mercedesamgf1.com/en/car/pu106a-hybrid/, November 2014.

[54] Nicola Terdich, Ricardo F Martinez-Botas, David A Howey, Colin D Copeland, and Aaron Costall. Off-road diesel engine transient response improvement by electrically assisted turbocharging. In *10th International Conference on Engines and Vehicles (ICE2011), Capri, Italy, September*, pages 11–15, 2011.

[55] Ian George Mervyn Thompson. *Investigations into the effects of Turbocompounding*. PhD thesis, Queen's University Belfast, 2012.

[56] Feng Tian, Guo Feng Ren, Bin Yan, Guo Qiang Ao, and Lin Yang. Optimization of hybrid turbocharger applied on common rail diesel engine with exhaust gas recirculation. *Applied Mechanics and Materials*, 246:84–88, 2013.

[57] Paolino Tona, Stéphane Venturi, and Richard Tilagone. Integrated powertrain control for a mild-hybrid urban vehicle with a downsized turbocharged cng engine. *Training*, 2011:11–04, 2008.

[58] Xi Wei, Pierluigi Pisu, Giorgio Rizzoni, and Stephen Yurkovich. Dynamic modeling of a hybrid electric drivetrain for fuel economy, performance and driveability evaluations. In *ASME 2003 international mechanical engineering congress and exposition*, pages 443–450. American Society of Mechanical Engineers, 2003.

[59] Hyoung-Jin Yoon and Se-Jin Lee. An optimized control strategy for parallel hybrid electric vehicle. Technical report, SAE Technical Paper, 2003.

[60] Qingning Zhang, Andrew Pennycott, and Chris J Brace. A review of parallel and series turbocharging for the diesel engine. *Proceedings of the Institution of Mechanical Engineers, Part D: Journal of Automobile Engineering*, 227(12):1723–1733, 2013.

[61] Dezong Zhao, Richard Stobart, Guangyu Dong, and Edward Winward. Real-time energy management for diesel heavy duty hybrid electric vehicles.

[62] Yuan Zhu, Yaobin Chen, Guangyu Tian, Hao Wu, and Quanshi Chen. A four-step method to design an energy management strategy for hybrid vehicles. In *American Control Conference, 2004. Proceedings of the 2004*, volume 1, pages 156–161. IEEE, 2004.

ETH
Eidgenössische Technische Hochschule Zürich
Swiss Federal Institute of Technology Zurich

Institute for Dynamic Systems and Control
Prof. Dr. R. D'Andrea, Prof. Dr. L. Guzzella

Title of work:

Optimal Control of a Hybrid Electric Vehicle with an Electrically Assisted Turbocharger

Thesis type and date:

Master Thesis, December 2014

Supervision:

Christian Naegele, Daimler AG
Pedro Macri-Lassus, Daimler AG
Dr. Tobias Nüesch, ETH Zurich

Student:

Name:	Achin Jain
E-mail:	ajain@student.ethz.ch
Legi-Nr.:	12-946-760
Semester:	4

Statement regarding plagiarism:

By signing this statement, I affirm that I have read the information notice on plagiarism, independently produced this paper, and adhered to the general practice of source citation in this subject-area.

Information notice on plagiarism:

http://www.ethz.ch/students/semester/plagiarism_s_en.pdf

Zurich, 22. 12. 2014: _____